HHS Public Access

Author manuscript

*Sci Transl Med*. Author manuscript; available in PMC 2021 August 09.

Published in final edited form as:

*Sci Transl Med*. 2021 February 10; 13(580): . doi:10.1126/scitranslmed.abc6894.

# Targeted immunotherapy for HER2-low breast cancer with 17p loss

**Yujing Li**[1,*], **Yifan Sun**[1,*], **Michael Kulke**[2], **Torsten Hechler**[2], **Kevin Van der Jeught**[1], **Tianhan Dong**[3], **Bin He**[4,5], **Kathy D. Miller**[6,7], **Milan Radovich**[6,8], **Bryan P. Schneider**[6,7], **Andreas Pahl**[2], **Xinna Zhang**[1,6,†], **Xiongbin Lu**[1,6,9,†]

[1]Department of Medical and Molecular Genetics, Indiana University School of Medicine, Indianapolis, IN 46202, USA.

[2]Heidelberg Pharma Research GmbH, Ladenburg 68526, Germany.

[3]Department of Pharmacology and Toxicology, Indiana University School of Medicine, Indianapolis, IN 46202, USA.

[4]Departments of Surgery and Urology, Immunobiology and Transplant Science Center, Houston Methodist Cancer Center, Houston Methodist Research Institute, Houston Methodist Hospital, Houston, TX 77030, USA.

[5]Department of Medicine, Weill Cornell Medicine of Cornell University, New York, NY 10065, USA.

[6]Indiana University Melvin and Bren Simon Cancer Center, Indiana University School of Medicine, Indianapolis, IN 46202, USA.

[7]Division of Hematology/Oncology, Department of Medicine, Indiana University School of Medicine, Indianapolis, IN 46202, USA.

[8]Department of Surgery, Indiana University School of Medicine, Indianapolis, IN 46202, USA.

[9]Indiana University Center for Computational Biology and Bioinformatics, Indiana University School of Medicine, Indianapolis, IN 46202, USA.

## Abstract

[†]Corresponding author. xz48@iu.edu (X.Z.); xiolu@iu.edu (X.L.).
[*]These authors contributed equally to this work.

**Author contributions:** Y.L., Y.S., X.L., and X.Z. designed the experiments. Y.S. and X.L. conducted bioinformatics and statistical analyses. T.D. and B.H. assisted in cell-based studies. K.V.d.J. provided technical support for immunological analyses. K.D.M., M.R., and B.P.S. provided guidance in analysis of clinical samples and databases. M.K., T.H., and A.P. synthesized and characterized ADCs. X.L., X.Z., and Y.L. wrote and revised the manuscript.

SUPPLEMENTARY MATERIALS
stm.sciencemag.org/cgi/content/full/13/580/eabc6894/DC1

**Competing interests:** X.L. has a U.S. patent (no. 10563204) on “Methods of treating cancer harboring hemizygous loss of TP53” licensed to Heidelberg Pharma AG. T.H. holds patents (WO2014135282A1, WO2016142049A1, WO2017149077A1, WO2018115466A1, WO2019030171A1, WO2019030173A1, WO2019057964A1, WO2019197654A1, and WO2020216947A1) in the field of amanitin-based ADCs.

**Data and materials availability:** All data associated with this study are present in the paper or the Supplementary Materials. The code of ICTD is deposited in Zenodo (DOI: 10.5281/zenodo.4313774). ADCs will be made available for the scientific community through contacting A.P. (andreas.pahl@hdpharma.com) and completion of a material transfer agreement.

The clinical challenge for treating HER2 (human epidermal growth factor receptor 2)–low breast cancer is the paucity of actionable drug targets. HER2-targeted therapy often has poor clinical efficacy for this disease due to the low level of HER2 protein on the cancer cell surface. We analyzed breast cancer genomics in the search for potential drug targets. Heterozygous loss of chromosome 17p is one of the most frequent genomic events in breast cancer, and 17p loss involves a massive deletion of genes including the tumor suppressor *TP53*. Our analyses revealed that 17p loss leads to global gene expression changes and reduced tumor infiltration and cytotoxicity of T cells, resulting in immune evasion during breast tumor progression. The 17p deletion region also includes *POLR2A*, a gene encoding the catalytic subunit of RNA polymerase II that is essential for cell survival. Therefore, breast cancer cells with heterozygous loss of 17p are extremely sensitive to the inhibition of POLR2A via a specific small-molecule inhibitor, α-amanitin. Here, we demonstrate that α-amanitin–conjugated trastuzumab (T-Ama) potentiated the HER2-targeted therapy and exhibited superior efficacy in treating HER2-low breast cancer with 17p loss. Moreover, treatment with T-Ama induced immunogenic cell death in breast cancer cells and, thereby, delivered greater efficacy in combination with immune checkpoint blockade therapy in preclinical HER2-low breast cancer models. Collectively, 17p loss not only drives breast tumorigenesis but also confers therapeutic vulnerabilities that may be used to develop targeted precision immunotherapy.

## INTRODUCTION

Cancer genomics analysis revealed that heterozygous deletion of chromosome 17p is one of the most prevalent events in many types of human cancer (1–4). Within the 17p deletion region is the tumor suppressor *TP53* (encoding p53), whose deletion or mutation has been long known as a primary tumorigenic driver (5). However, it remains unclear whether the deletion event, which often includes as many as 908 genes with 346 protein coding genes, affects tumorigenesis besides *TP53* loss alone (6, 7). A recent study revealed that deletion of *Eif5a* and *Alox15b* in mouse 11B3 (syntenic to human 17p13.1) contributes to the malignancy of lymphoma and leukemia in cooperation with *Trp53* (mouse *TP53*) deletion (6). Because p53 aberrancy promotes proliferation, metabolism, and metastasis, enormous efforts have been made to restore p53 activity for therapeutic development. Small chemical compounds have been developed to block the MDM2-p53 or MDMX-p53 interaction (8). However, this strategy is only applicable to cancers expressing wild-type p53, but not for cancers expressing mutant p53 or no p53, a common feature of human cancers. Heterozygous deletion of 17p results in a reduced dosage of the *TP53*-neighboring essential genes that may not contribute to cancer development. However, the loss of such essential genes renders cancer cells highly vulnerable to further inhibition of these genes (2, 3, 7). We identified a *TP53*-neighboring gene, *POLR2A*, as a potential drug target, which encodes the catalytic subunit of RNA polymerase II (RNAP2) complex (2, 3, 7). Because RNAP2 is in charge of mRNA synthesis, a function required for cell survival, complete knockout of *POLR2A* is lethal to any type of cells. Whereas heterozygous loss of *POLR2A* in cancer cells has minimal impact on cell proliferation and survival, it creates therapeutic vulnerability in cancer cells containing such genomic defects.

As a powerful prognostic marker in node-positive patients with breast cancer, human epidermal growth factor receptor 2 (HER2) overexpression is associated with increased tumor recurrence and decreased patient survival (9–11). In the clinic, HER2 immunohistochemistry (IHC) staining has been the most widely used approach for evaluating HER2 as a predictor of response to anti-HER2 therapy (12). According to current clinical guidelines, IHC results score HER2 status as positive (3+), equivocal (2+), and negative (0 or 1+) for breast cancer cases (12). Despite low to medium levels of HER2 proteins, breast tumors with HER2 1+ or 2+ are not considered as positive for HER2 overexpression, and such tumors are believed unlikely to respond to anti-HER2 therapy (13). Results of clinical trials also showed that treatment with trastuzumab (anti-HER2 antibody) or T-DM1 (ado-trastuzumab emtansine) did not benefit patients with HER2-low breast cancer (14, 15). However, a recent HER2-targeted antibody-drug conjugate (ADC), trastuzumab deruxtecan (T-DXd), demonstrated promising preliminary antitumor activity in patients with HER2-low breast cancer (16). These data, as well as the high efficacy and specificity of anti-HER2 agents, suggest that targeting HER2 could be a feasible approach for HER2-low breast cancer.

## RESULTS

### 17p loss is frequent and correlated with poor immune response in breast cancer

The heterozygous loss of *TP53* and 17p was identified in a number of human cancers (2, 3, 6, 7). We sought to develop a therapeutic approach against breast cancer harboring 17p loss. To this end, we first assessed the distribution of various genomic attributes along the genetic map of breast cancer from The Cancer Genome Atlas (TCGA) and Molecular Taxonomy of Breast Cancer International Consortium (METABRIC) cohorts (Fig. 1A). Among the most frequent chromosomal amplification and deletion events is the heterozygous loss of 17p, which occurs in 51.6% of human breast cancers (Fig. 1A). Most of the deletion events span over the whole arm of 17p. The complete 17p loss is frequently detected in each subtype of breast cancer, including 31.9% in estrogen receptor $(ER)^+$/progesterone receptor $(PR)^+$ breast cancer, 41.9% in triple-negative breast cancer (TNBC), and 44.4% in $HER2^+$ breast cancer (Fig. 1B and fig. S1A), suggesting that this event is not associated with particular breast cancer subtypes. Clinical data analysis revealed that the complete 17p loss is correlated with poor overall survival of patients with breast cancer ($P = 0.00002$) and in TNBC ($P = 0.04$; Fig. 1C and fig. S1B). To understand the biological relevance of 17p loss, we analyzed the gene expression profiles in $17p^{intact}$ versus $17p^{loss}$ TNBC cases (fig. S1C). The gene set enrichment analysis (GSEA) demonstrated that up-regulated genes in the $17p^{loss}$ TNBC are enriched in cell cycle regulation, DNA replication, and cell metabolism pathways, whereas those down-regulated genes are often associated with immune response and modulation of tumor cells as well as tumor-stromal interaction (Fig. 1D). We used the inference of cell types and deconvolution (ICTD) algorithm to assess the correlation of 17p loss with $CD8^+$ T cell infiltration and cytotoxicity in TNBC. The ICTD allows for an unbiased inference of cell proportions and activities from bulk tissue RNA sequencing (RNA-seq) data (17). In comparison with the $17p^{intact}$ TNBC, significantly fewer infiltrating $CD8^+$ T cells ($P = 9.2 \times 10^{-6}$) and putative cytotoxicity ($P = 0.00011$) were observed in the $17p^{loss}$ TNBC (Fig. 1E), which was consistent with the results of CIBERSORT

(Cell-type Identification By Estimating Relative Subsets Of known RNA Transcripts) (fig. S1D) (18). Furthermore, we confirmed the reduced infiltration and cytotoxicity of $CD8^+$ T cells in $17p^{loss}$ TNBCs by immunostaining analysis of a TNBC tissue microarray with granzyme B (GZMB) and CD8 antibodies (fig. S1E). Comprehensive immune profiling analysis using a series of biomarkers for T cell activity and subtypes suggested that most of the T cell activity markers were down-regulated in $17p^{loss}$ TNBCs in comparison with those in $17p^{intact}$ TNBCs. Moreover, down-regulation of these T cell markers is mostly associated with poor patient survival (fig. S2). In addition, a panel of immune pathways such as wound healing, interleukin-2 (IL-2), CD8_TCR, B cell receptor, and antigen presentation pathways were also significantly ($P < 0.05$) down-regulated in the $17p^{loss}$ TNBCs (fig. S3). These results collectively suggest that 17p loss is likely involved in immune suppression or evasion of the tumor.

## Trastuzumab conjugated to α-amanitin is effective in killing HER2-low breast cancer cell lines with 17p loss

The natural compound α-amanitin is a highly specific inhibitor for POLR2A with a $K_d$ (dissociation constant) value of ~1 nM (19). The approach of using α-amanitin–based ADCs disrupts its interaction with the hepatocyte-specific organic anion transporting polypeptide 1B3 (OATP1B3) transporter and, thus, markedly reduces liver toxicity and increases tumor-targeting specificity (3, 20). We sought to develop α-amanitin–conjugated trastuzumab (T-Ama) for treating HER2-low breast cancer, particularly HER2-low TNBC. To this end, we first determined the percentage of HER2-low TNBC cases that also harbor 17p loss. Analysis of TCGA breast cancer dataset showed that 32.2% of HER2-low TNBCs (HER2 1+ and 2+) are $17p^{loss}$, similar to the percentage (39%) of $17p^{loss}$ TNBC cases in the tumor microarray analysis (Fig. 2A and fig. S4, A to C). To synthesize T-Ama, we covalently conjugated an α-amanitin compound with a stable linker to the introduced cysteine residue on position 265 in the heavy chains of trastuzumab with the drug-to-antibody ratio of ~2.0 (fig. S4D). T-Ama showed the same binding capacity as trastuzumab to HER2-expressing cell lines (fig. S4E). To assess the targeting specificity and tumor cell killing efficacy of T-Ama, a panel of $17p^{intact}$ and $17p^{loss}$ cell lines were identified and validated by copy numbers of the genes in the 17p region (fig. S5A). Heterozygous loss of 17p leads to reduced POLR2A expression (fig. S5B) and increased sensitivity to α-amanitin (fig. S5C), which is consistent with previous reports in other types of cancer (2, 3, 7). We evaluated a number of TNBC cell lines (MDA-MB-453, HCC1143, HCC1187, HCC38, BT20, and HCC70) that have low expression of HER2 determined by flow cytometry (Fig. 2B). The number of HER2 molecules on the surface of these HER2-low cell lines was calculated by comparing the median fluorescence intensity (MFI) of HER2 of the samples to that of the microspheres with known antibody binding capacity (ABC). We found that the number of HER2 molecules on HER2-low cell lines was 8- to 40-fold less than those on the HER2-positive (IHC 3+) cell lines (BT474 and SKBR3) (21). In the $17p^{intact}$ cell lines, the tumor cell killing activity of T-Ama was dependent on the expression of HER2 on the cell surface. Whereas $HER2^+$ cell lines AU565 and BT474 exhibited high sensitivity to the treatment of T-Ama or T-DM1, $17p^{intact}$ cell lines with low HER2 were insensitive to either of these two ADCs (Fig. 2C), suggesting that HER2 expression is the primary factor for the response of $17p^{intact}$ breast cancer cells to the treatment of trastuzumab-based ADCs.

By contrast, T-Ama had markedly higher cytotoxicity on the $17p^{loss}$ breast cancer cells with low expression of HER2 than T-DM1 ($P = 0.0148$; Fig. 2D). The half-maximal inhibitory concentration ($IC_{50}$) of T-Ama was 20- to 200-fold lower than the $IC_{50}$ of T-DM1 on the same cell lines. The cell lines with no HER2 such as MDA-MB-231 and MDA-MB-468 were insensitive to either of these two ADCs, regardless of their 17p status. To test the antitumor effect of T-Ama in vivo, HER2-low TNBC cell lines BT20 ($17p^{intact}$) and HCC70 ($17p^{loss}$) were orthotopically implanted into the fourth mammary gland of immunodeficient nude (Nu/J) mice. No substantial tumor growth or overall survival differences were observed between control and T-Ama–treated mice bearing $17p^{intact}$ BT20-derived tumors (Fig. 2E). In contrast, administration of T-Ama even at very low doses (0.1 to 0.5 mg/kg) significantly ($P < 0.001$) inhibited the growth of HCC70-derived tumors, and treatment of T-Ama at 2.0 mg/kg resulted in complete tumor regression (Fig. 2F). Treatment with T-DM1 (2.0 mg/kg) had no effect on tumor growth in either BT20- or HCC70-derived tumors (fig. S5D).

## 17p knockout sensitizes HER2-low TNBC cells to T-Ama treatment

To exclude genetic difference across cell lines, we used the CRISPR (clustered regularly interspaced short palindromic repeat)–Cas9 system (22, 23) to delete one copy of 17p from *WDR81* to *MAP2K3* with the size of ~19.6 Mb in HS578T cells. DNA sequencing of the clones revealed the fusion of the remaining *WDR81* and *MAP2k3* genes (Fig. 3A and fig. S6A). Western blotting and reverse transcription polymerase chain reaction (RT-PCR) analyses further confirmed the heterozygous loss of 17p in the positive cell colonies (fig. S6, B and C). Heterozygous deletion of 17p sensitized HS578T cells to α-amanitin treatment with an $IC_{50}$ value of 0.2 μg/ml, which is 10-fold lower than that of $17p^{intact}$ HS578T cells ($P < 0.001$; fig. S6D). Next, we used the $17p^{intact}$ and $17p^{loss}$ HS578T cells to generate a series of isogenic cell lines with stable HER2 expression levels (0, 1+, 2+, and 3+) (fig. S6, E and F). Whereas the $17p^{intact}$ HS578T cells display similar sensitivity to T-Ama and T-DM1 with same HER2 status (Fig. 3B), the $17p^{loss}$ HS578T cells were more sensitive to the treatment of T-Ama in comparison with their isogenic $17p^{intact}$ counterparts with same HER2 status ($P < 0.001$). In the $17p^{loss}$ cell lines with HER2-low (1+ or 2+) status, T-Ama exhibited at least 30-fold greater cytotoxicity than that of T-DM1 (Fig. 3C). We next ectopically expressed POLR2A in $17p^{loss}$ HS578T cells (fig. S6G). Ectopic expression of POLR2A partially restored their resistance to the T-Ama treatment ($P = 0.0012$; Fig. 3D). Because of the lack of HER2 expression, normal human mammary epithelial cells (MC-F10A), fibroblasts (IMR90 and WI38), and hepatocyte-derived cancer cells (HepG2 and Huh7) are insensitive to either T-Ama or T-DM1 treatment (fig. S7).

## T-Ama exhibits greater activity than T-DM1 in inhibiting $17p^{loss}$/HER2-low TNBC growth

To compare the antitumor activity of T-Ama and T-DM1 in vivo, we orthotopically implanted HER2-low $17p^{intact}$ or $17p^{loss}$ HS578T cell lines into the fourth mammary gland of Nu/J mice. HER2 expression level of the tumors was scored as 1+ by independent pathological analysis (fig. S8). Treatment of T-Ama at 2 mg/kg did not reduce tumor burden or extend survival in mice bearing $17p^{intact}$/HER2-low HS578T-derived tumors ($P = 0.919$; Fig. 4A). In contrast, T-Ama treatment inhibited the growth of the tumors derived from the isogenic $17p^{loss}$/HER2-low HS578T cells ($P < 0.0001$) and extended survival ($P < 0.001$; Fig. 4B). T-DM1 did not show any notable activity on either $17p^{intact}$ or $17p^{loss}$

tumors with low expression of HER2 (Fig. 4, A and B). Further, whereas a single dose of T-Ama (2.0 mg/kg) inhibited both the $17p^{intact}$/HER2-low and $17p^{loss}$/HER2-low tumor in the patient-derived xenograft (PDX) model (Fig. 4, C and D), a single dose of T-Ama (0.5 mg/kg) sufficiently controlled tumor burden ($P < 0.001$) in the $17p^{loss}$/HER2-low PDX (Fig. 4D). Collectively, T-Ama demonstrated specific efficacy in killing HER2-low breast cancer with 17p loss.

## T-Ama treatment does not result in overt toxicity in vivo

In terms of T-Ama toxicity, no signs of systemic intolerance such as abnormal death, body weight changes, or tissue histological changes were observed in the T-Ama– or T-DM1–treated groups (fig. S9). No notable changes in liver-relevant biochemical parameters including aspartate aminotransferase (AST), alanine aminotransferase (ALT), and alkaline phosphatase (AP) were seen after application of T-Ama (8.0 mg/kg) (fig. S9B). A tolerability study using a nonbinding control antibody (anti-digoxigenin) conjugated to α-amanitin with the same linker was also conducted in nonhuman primates (female cynomolgus monkeys) (fig. S10). The nontargeting α-amanitin ADC was applied at doses from 0.3 to 3.0 mg/kg. No notable increase was observed in liver transaminases (AST and ALT) and lactate dehydrogenase at the dose up to 1.0 mg/kg, whereas only transient increase was seen at the high dose of 3.0 mg/kg. The results suggest that the T-Ama was well tolerated after administration to nonhuman primates.

## α-Amanitin treatment induces immunogenic cell death in breast cancer cell lines

Previous studies reported that α-amanitin induced cell death primarily by apoptosis (24). We confirmed that apoptosis, but not necrosis, is the main death mechanism induced by α-amanitin in breast cancer cells (fig. S11). Next, we sought to determine whether α-amanitin induces immunogenic cell death (ICD). ICD is a form of cell death that induces an effective antitumor immune response via dendritic cells (DCs) and consequent activation of specific T cell response (25). We examined whether the α-amanitin treatment elicits ICD characteristic damage-associated molecular patterns (DAMPs) in the HER2-low MDA-MB-453 and HCC70 breast cancer cells. Three major ICD markers including calreticulin, adenosine triphosphate (ATP), and high-mobility group box 1 (HMGB1) were assessed in the cells treated with α-amanitin, positive control doxorubicin (a known ICD inducer) or negative control C2 ceramide (Crm) (26, 27). The results demonstrated that treatment of α-amanitin induced DAMPs including calreticulin ($P < 0.0001$), ATP ($P = 0.0001$), and HMGB1 ($P = 0.0007$) in MDA-MB-453 cells and HCC70 cells (Fig. 5A and fig. S12A) under the $IC_{50}$ dose of indicated drugs (fig. S12B). ICD is coupled to the induction of type I interferons (IFNs) that act in an autocrine fashion on cancer cells, thereby increasing their immunogenic potential (28–30). In addition, ICD also causes the release of pathogen response–like chemokines (31). Therefore, we measured the induction of type I IFN and IFN-stimulated genes (*MX1*, *OAS2*, and *RSAD2*), as well as the pathogen response–like chemokine genes (*CXCL1*, *CCL2*, and *CXCL10*) upon α-amanitin treatment. Our data showed that both doxorubicin and α-amanitin treatment significantly ($P < 0.0001$ to $P < 0.05$) induced RNA expression of these genes in MDA-MB-453 and HCC70 cells (fig. S12, C and D). It has also been established that ICD of cancer cells promotes DC maturation (32). Therefore, we assessed the effect of α-amanitin–induced ICD on DC maturation. Bone marrow was

isolated from C57BL/6 mice and subsequently differentiated to immature bone marrow–derived DCs (BMDCs) (fig. S12E). BMDCs were then cocultured with mouse EO771 breast cancer cells pretreated with $IC_{50}$ doses of Crm, doxorubicin, or α-amanitin (fig. S12F). As a positive control for DC maturation, BMDCs were treated with the proinflammatory Toll-like receptor 4 ligand, lipopolysaccharide (LPS). Flow cytometry analysis of BMDCs demonstrated that coculture with EO771 cells preexposed to α-amanitin significantly ($P < 0.01$) induced up-regulation of the costimulatory ligands major histocompatibility complex II (MHC-II)$^+$CD80$^+$ and MHC-II$^+$CD86$^+$ (Fig. 5, B and C) on BMDCs when compared with coculture with mock-treated or Crm-treated EO771 cells. The level of maturation of BMDCs was associated with increasing concentrations of α-amanitin (fig. S13, A and B). To evaluate BMDC maturation, we analyzed cytokines, including IL-12, tumor necrosis factor–α (TNFα), IL-1β, IL-6, IL-10, and transforming growth factor–β (TGFβ) secreted by BMDCs. BMDCs were cocultured for 24 hours with EO771 cells pretreated with Crm, doxorubicin, or α-amanitin. The dead EO771 cells were then removed, and a new medium was replaced. The cytokines in the supernatant of BMDCs were analyzed. Doxorubicin- or α-amanitin–treated tumor cells stimulated BMDCs to release cytokines such as IL-12, TNFα, IL-1β, and IL-6 but not IL-10 or TGFβ in vitro. As a control, Crm-treated tumor cells failed to stimulate BMDCs to release any of the above cytokines (Fig. 5D). To assess the ICD effect in vivo, we conducted a vaccination assay. Cell death was induced in EO771 cells with the $IC_{50}$ dose of indicated drugs. The resulting dead and dying EO771 cells were then inoculated subcutaneously into the left lower flank of C57BL/6 mice. Ten days after vaccination, the mice were inoculated on the opposite lower flank with live EO771 cells. If ICD occurs, then the mice should demonstrate protection against a subsequent challenge with live EO771 tumor cells (fig. S13C) (33). Whereas phosphate-buffered saline (PBS) or tumor cells treated with Crm did not provide protection against secondary EO771 tumor challenge, the mice vaccinated with doxorubicin-or α-amanitin–treated cells had a significant survival benefit ($P < 0.001$; Fig. 5E). T-Ama–treated cells also protected mice from rechallenge and extended survival ($P < 0.001$), suggesting that the ICD induced by α-amanitin is not affected by the antibody conjugation (fig. S13D). Blocking IFNα/β receptor subunit 1 (IFNAR1) or HMGB1 abolished the ability of T-Ama–treated cells to protect mice from the rechallenge, highlighting the role of DAMPs and type I IFN signaling in α-amanitin–induced ICD (fig. S13, E and F).

## T-Ama and immune checkpoint blockade control tumor burden in mice bearing subcutaneous HER2-low tumors

Given the immune engagement observed for α-amanitin in T-Ama, we reasoned that T-Ama could induce an efficient antitumor immune response, and the combination of T-Ama treatment with immune checkpoint blockade therapy may help control tumor burden in HER2-low breast cancer. To test this hypothesis, we transplanted human HER2-expressing mouse EO771 cells into C57BL/6-Tg(WapHER2) transgenic mice. This mouse strain expresses human HER2 under mouse *Wap* (whey acid protein) promoter that directs mammary gland–specific expression (34). They do not develop spontaneous tumors but are tolerant to human HER2-associated antigen. We also generated an isogenic HER2-low (equivalent to HER2 1+) cell line derived from EO771 with heterozygous loss of chromosome 11B, which is syntenic to human chromosome 17p (fig. S14, A to E). Loss

of mouse chromosome 11B (a 16-Mb region between *Flcn* and *Crk* or between 11B2 and 11B5) was generated to model the 17p loss in human breast cancer (35). The 11B loss increased the sensitivity of HER2-low–expressing EO771 cells to the treatment of α-amanitin and T-Ama (fig. S14, F and G). We next assessed the therapeutic responses of HER2-low and $11B^{loss}$ EO771 orthotopically implanted into the fourth mammary gland of the C57BL/6-Tg(WapHER2) mice to the treatment of T-Ama alone or in combination with programmed cell death protein 1 (PD-1)–blocking antibody. Whereas PD-1 blockade treatment had minimal antitumor activity, the T-Ama (5 mg/kg) treatment alone inhibited the tumor growth ($P < 0.0001$; Fig. 6A). Greater tumor growth control ($P < 0.0001$), as well as extended survival ($P = 0.007$) of the tumor-bearing mice, was observed when T-Ama was added to the PD-1 blockade treatment (Fig. 6, A and B). To examine the T-Ama–induced immunological changes, we harvested the mammary tumors 30 days after tumor implantation for mass cytometry (CyTOF) analysis (Fig. 6C and table S1). T-Ama treatment alone or in combination with PD-1 antibody led to enhanced infiltration of immune cells, particularly $CD8^+$ T effector cells and conventional $CD4^+$ T cells in comparison with single-agent treatment of PD-1 antibody or control treatment (Fig. 6D and fig. S15A), suggesting that treatment promotes an antitumor microenvironment. To determine whether $CD4^+$ and $CD8^+$ T cell populations are responsible for the immunological effect of T-Ama, we depleted mice of both $CD4^+$ and $CD8^+$ T cells. The depletion antibodies were administered intraperitoneally before tumor inoculation and every 3 days thereafter until the tumors reached 1000 $mm^3$ or the mice became moribund. The antitumor effect for T-Ama was significantly ($P < 0.001$) dampened upon $CD4^+$ and $CD8^+$ depletion (fig. S15B). We further characterized tumor-infiltrating T cells in control and treated mice (table S2). We observed an increase in activation markers (IL-2) for both $CD4^+$ and $CD8^+$ tumor-infiltrating T cells after T-Ama or combination treatment (fig. S15, C and D). We also observed signs of T cell exhaustion based on the markers PD-1, T cell immunoglobulin and mucin domain–containing protein 3 (TIM3), and lymphocyte-activation gene 3 after T-Ama or combination treatment (Fig. 6, E and F, and fig. S15, C and D). Although those T cells display exhaustion markers, treatment with T-Ama as a single agent or in combination led to increased expression of TNFα and IFN-γ in $CD8^+$ T cells (Fig. 6G and fig. S16, A and B) as well as increased perforin 1 (PRF1) and GZMB signals in the tumor sections (fig. S16, C and D), indicating a proinflammatory phenotype. The $CD3^+$ T cells isolated from the T-Ama–treated tumors also secreted higher concentrations of TNFα and IFN-γ than those from the tumors with control or PD-1 single-agent treatment ($P < 0.0001$; Fig. 6H). No overt toxicity was observed on the mouse mammary glands in the T-Ama treatment group as evidenced by the normal mammary gland architecture consisted of ducts lined by a single layer of simple cuboidal epithelial cells supported by a layer of myoepithelial cells, evident ductal lumens, and uniform adipocytes throughout the sections (fig. S17A). We also noticed that the HER2 protein levels in tumors are significantly ($P < 0.001$) lower in the T-Ama and combo treatment groups as compared to control group or PD-1 single-agent treatment groups, suggesting that further reduced HER2 expression may be a possible mechanism of resistance against T-Ama (fig. S17, B and C). Together, the results provide insight into the mechanisms of T-Ama's therapeutic activity and a rationale for potential therapeutic combination strategies with immune checkpoint blockade therapy.

## DISCUSSION

HER2-low breast cancer is a molecularly diverse and clinically heterogeneous disease. TNBC is particularly challenging in cancer therapeutics. Patients with TNBC do not benefit from hormonal or trastuzumab-based therapy because this type of cancer neither expresses the target ER or PR nor produce a high level of HER2 protein. Surgery and chemotherapy, individually or in combination, have been the only available treatment options for most patients. Efforts have been made to develop effective targeted therapies to improve clinical outcomes in TNBC. The first approved immunotherapy for breast cancer is the programmed death ligand 1 (PD-L1) inhibitor atezolizumab and nab-paclitaxel (nanoparticle albumin–bound paclitaxel) as first-line therapy for unresectable locally advanced or metastatic TNBCs that express PD-L1 in 1% or greater of tumor cells (36). Furthermore, results from clinical trials using various immune checkpoint inhibitors are mixed (37, 38). There is an urgent need to develop additional targets, combinational therapies, treatment strategies, and prognostic biomarkers for patients diagnosed with TNBC.

Breast cancer genomics revealed that heterozygous deletion of 17p is a frequent genomic event in TNBC. Whereas p53 aberrancy in the deletion region promotes proliferation, metabolism, and metastatic potential of the TNBC cells, we found that 17p loss is tightly correlated with poor cytotoxicity of tumor-infiltrating lymphocytes and poor clinical outcomes in patients with TNBC. A selective advantage for 17p loss in tumor progression may be attributed to the combined impact of many deleted genes in the region. To accelerate the translational development of POLR2A inhibitors, we have been attempting to develop ADCs with cytotoxic α-amanitin as drug payload. This approach simultaneously overcomes two bottlenecks in developing POLR2A inhibitors as a cancer drug: systematic toxicity and targeting specificity. One of key factors for a successful ADC is to identify a monoclonal antibody with high specificity and effectivity for TNBC. Sacituzumab govitecan (IMMU-132, Immunomedics), an anti-Trop2 antibody conjugated to SN-38 seems to be promising in treating TNBC (39). In this study, we used trastuzumab to develop α-amanitin–based ADC for treating HER2-low TNBC because a high percentage (80%) of TNBC is HER2 1+ or 2+ and because trastuzumab has been used in the clinic with great safety as first-line standard care for $HER2^+$ breast cancer (40). Furthermore, T-DM1, emtansine-conjugated trastuzumab, was also approved for treating $HER2^+$ metastatic breast cancer with great tolerability and safety (41). Last, α-amanitin greatly induces ICD and thus promotes the efficacy of immune checkpoint blockade therapy. Overall, T-Ama appears to be a drug candidate with strong clinical potential for HER2-low breast cancer with great tolerability and low off-target toxicity.

As an emerging cancer treatment modality, a number of ADCs have entered clinical trials (42, 43). However, most of ADCs are based on a few toxic compounds, such as maytansines (in T-DM1) and irinotecan (in T-DXd), and their mechanisms of action are often limited to disruption of microtubules or DNA replication. The clinical efficacy of these ADCs could suffer from limited activity in resistant cancer cells or cancer stem cells. Accordingly, the use of new drugs that function via alternative toxicity mechanisms will potentially enhance the therapeutic activity of ADCs. As one of the recently developed drug conjugates for ADCs, α-amanitin has advantages over other toxins due to its unique mode of action

and molecular characteristics (3, 44). In particular, as the most potent inhibitor of cellular transcription, α-amanitin targets the specific vulnerability of cancer cells conferred by genomic loss of *POLR2A* and 17p. This increases therapeutic index by selectively killing cancer cells with this genomic aberrancy and reduces potential toxicity in healthy tissues. Inhibition of POLR2A by α-amanitin leads not only to apoptosis of dividing cancer cells with 17p loss but also to that of slowly growing or quiescent cancer cells, as often observed in metastatic breast cancer. About 15% of breast cancers are HER2 positive, but as many as 45% of breast cancers have low levels of HER2 (13). Although the latter are not considered candidates for treatment of trastuzumab alone, this study showed that T-Ama is effective in killing HER2-low TNBC cells harboring 17p loss.

A limitation of this study is that, despite its superior antitumor activity on HER2-low breast cancer when used alone or in combination with PD-1–based immunotherapy, T-Ama is generally ineffective in the $17p^{intact}$ tumors. This will limit its clinical utility to $17p^{loss}$ breast cancer. Further, the drug-to-antibody ratio of T-Ama is ~2 at its current version in comparison with ~4 in T-DM1 and ~8 in T-DXd, suggesting that there is room for improvement in terms of drug-antibody conjugation. A final limitation is that unlike other candidate drug conjugates, such as maytansines and irinotecan, the pharmacological characteristics and toxicity of α-amanitin in human body have yet to be studied. Because trastuzumab does not bind to rodent erb-b2 receptor tyrosine kinase 2 (ERBB2), further drug safety studies and future clinical trials with T-Ama will help address these questions.

The present study identifies a targeted immunotherapy approach for HER2-low breast cancer harboring 17p loss. As one of the most difficult to treat subtypes of breast cancer, there is a great need to identify new treatment options for TNBC. Given the high frequency of 17p loss in the HER2-low TNBCs, this work has potential application in both clinical trials and disease prognosis. As a single agent or in combination with immune checkpoint blockade, T-Ama shows great promise in treating patients with HER2-low breast cancer.

## MATERIALS AND METHODS

### Study design

The goal of this study was to develop a targeted treatment regimen for HER2-low (IHC 1+ and 2+) breast cancers, particularly TNBCs, which harbor heterozygous loss of 17p. We developed an ADC using T-Ama and tested its activity in a series of breast cancer cells with different levels of HER2 (0, 1+, 2+, and 3+) and different 17p statuses in vitro and in xenograft tumor models. The toxicity of T-Ama was evaluated in both mice and monkeys. A group of three cynomolgus monkeys received a nonbinding control antibody (anti-digoxigenin) conjugated to α-amanitin intravenously (slow bolus) in escalating doses, and serum was obtained at indicated time points. Animals were monitored over time for biochemical and hematological blood parameters, body weight, food consumption, clinical signs, and mortality. Our bioinformatic analysis revealed that $17p^{loss}$ TNBCs display low immune cell infiltration and compromised $CD8^+$ T cell cytotoxicity. We found that the T-Ama treatment triggered ICD and, thus, enhanced immune response against tumors. We established a syngeneic mouse breast tumor model to test whether the T-Ama treatment enhanced the efficacy of immune checkpoint blockade therapy. The effects of

T-Ama treatment on the immune profiles in TNBC tumors were analyzed by CyTOF. All in vitro assays were performed with at least duplicate samples and were repeated in three independent experiments. In vivo studies were performed using 5- to 6-week-old Nu/J, C57BL/6, and C57BL/6-Tg(WapHER2) mice. The number of mice used in each experimental group was determined on the basis of statistical power analysis to render statistical significance of the experimental data between different experimental groups and ranged from four to eight mice per group. Before treatment, mice were randomized on the basis of tumor volume to ensure evenly distributed average tumor sizes across each group. Mouse survival end points were based on the maximum tumor volume allowed (1000 $mm^3$). Investigators were blinded when monitoring tumor growth and mouse survival. No samples were excluded from the study. All mouse studies were performed under protocols approved by the Institutional Animal Care and Use Committee and the institutional review board of Indiana University School of Medicine. The mice were housed in microisolator cages in the animal facility that is specific pathogen free. All mice were fed standard normal chow diet (Teklad Diets 2018SX) ad libitum and housed under controlled temperature and 12-hour light/12-hour dark cycle conditions. The mice were under the general supervision of experienced veterinarians and were attended and monitored at least daily by a trained animal care technician.

### Breast cancer transcriptomics data analysis

For the bioinformatics analysis, we used datasets of breast cancer samples from the TCGA database (1091 patients) and METABRIC cohort (1904 patients), including data from 115 patients with TNBC in TCGA and 299 patients with TNBC in METABRIC. RNA-seq data were normalized by FPKM (Fragments Per Kilobase of transcript per Million mapped reads). We performed differential expression analysis for $17p^{loss}$ and $17p^{intact}$ TNBC (METABRIC, 251 patients with TNBC) and identified two sets of differentially expressed genes using the Limma R package (45) with threshold set at $P < 0.05$ and $|\log_2$ fold change$| > 0.25$ (*t* test). We next conducted GSEA for these two sets of differentially expressed genes (down-regulated genes and up-regulated genes) to identify the underlying function of gene sets. The annotated gene sets (file c2 canonical gene sets version 6) were chosen for the reference gene sets. A gene size of ≥100, a *P* value of Fisher's exact test of <0.05, and a false discovery rate (FDR) of <0.01 were set as the cutoff criteria.

### Deconvolution analysis for human breast cancer microenvironment

We used our recently developed deconvolution method, ICTD, to access cell proportions of T cells (17). Specifically, ICTD identifies dataset for specific cell types and uniquely expressed gene markers to optimize the estimation of cell proportion. In the collected TNBC tissue transcriptomics data, we identified high coexpression correlation among CD2, CD3D, CD3E, CD3G, CD8A, CD247, IL2 inducible T cell kinase (ITK), and GZMK genes. The first eigen vector of the expression profile of these genes was used to estimate the relative proportion of total CD8 T cells in each sample. We further examined the T cell cytotoxicity by specific marker genes [CD8A, Src like adaptor 2 (SLA2), GZMA, GZMB, GZMH, PRF1, and natural killer cell granule protein 7 (NKG7)] that were highly coexpressed in the samples with high predicted level of total T cells. The first eigen vector of the expression profile of these genes was used to estimate the whole-tissue cytotoxicity level in the patient

samples. We also used CIBERSORT to verify our results from ICTD and to predict the relative proportion of tumor-infiltrating immune cells. The code of ICTD is deposited in Zenodo (DOI: 10.5281/zenodo.4313774).

### Chromosome 17p copy number alteration analysis

Copy number alteration (CNA) data were downloaded from TCGA database (1080 patients with breast cancer, including 112 patients with TNBC) and METABRIC database (2173 patients with breast cancer, including 320 patients with TNBC). The 17p deletion pattern was defined by patient sample clustering in the heatmap of 17p CNA. R 3.6.3 statistical platform was used to process the hierarchical cluster analysis, and TNBC samples were classified into three main groups: 17p loss, 17p intact, and 17p partial loss. The Circos plot was generated by Circos package 0.69.9, and the pie chart was generated using webr (PieDonut) R package (46). Kaplan-Meier survival analysis was conducted by the “survival” R package after combining the overall survival of patients with breast cancer from the TCGA and METABRIC cohorts.

### Tissue culture and tissue microarray

Human breast cancer cell lines MCF10A, MDA-MB-231, MCF7, HS578T, HCC1143, BT20, BT474, AU565, MDA-MB-468, T47D, HCC70, HCC38, ZR751, HCC1187, MDA-MB-453, HCC1149, UACC812, SKBR3, and ZR7530 were purchased from the American Type Culture Collection. JIMT-1 cell line was purchased from the Leibniz Institute. All the cell lines were maintained under standard conditions specified by the manufacturer and were tested negative for mycoplasma contamination using a mycoplasma detection kit (Lonza). Breast cancer tissue microarray BR1901 were obtained from Biomax and included 95 patient samples of which 83 were TNBC.

### DAMP analysis

Cell death was induced with the $IC_{50}$ dose of Crm, doxorubicin, and α-amanitin. Cell death was confirmed by annexin V (#640906, BioLegend) and propidium iodide (P4170, Sigma-Aldrich) staining, followed by flow cytometry. Briefly, Cells were washed twice with cold PBS and resuspended in 100 μl of annexin V binding buffer (#422201, BioLegend). Five microliters of fluorescein isothiocyanate (FITC) annexin V and 10 μl of propidium iodide (50 μg/ml) were added to the samples with incubation for 15 min at room temperature in the dark. Four hundred microliters of binding buffer was added to the sample after incubation, and the samples were immediately analyzed by flow cytometry. To analyze calreticulin exposure on the cell surface, cells were collected and washed with ice-cold PBS containing 0.5% bovine serum albumin (BSA) and 0.02% sodium azide. After washing, cells were resuspended in PBS with anti-calreticulin antibody or isotype immunoglobulin G (IgG) for 40 min at 4°C and then resuspended in 200 μl of ice-cold PBS buffer and stained with propidium iodide. Last, the samples were analyzed by flow cytometry on a BD FACSAria. Analysis was performed using FlowJo software (v.10.6.2). The MFI of calreticulin was determined in propidium iodide–negative cells. To analyze ATP release, MDA-MB-453 and HCC70 were treated as described above, followed by incubation with medium containing 2% fetal bovine serum (FBS) for 24 hours. The supernatants were collected and centrifuged at 15,000 rpm at 4°C for 3 min. The supernatants were immediately used for ATP

measurements with analysis performed using the ENLITEN ATP Assay System (FF2000, Promega) as described by the manufacturer. To measure extracellular HMGB1, after the indicated treatment, supernatant was collected and centrifuged to remove floating cells. The HMGB1 in the supernatant was detected using an enzyme-linked immunosorbent assay (ELISA) kit (IBL, Hamburg) according to the manufacturer's instruction.

## Antibodies and reagents

For immunoblotting (IB) assay, antibodies were diluted in tris-buffered saline with 0.1% Tween 20 containing 5% BSA. For flow cytometry assay, antibodies were diluted in PBS containing 0.5% BSA. For IHC assay, antibodies were diluted in PBS containing 5% BSA. Anti-POLR2A antibody (sc-47701; 1:5000 diluted for IB and 1:200 diluted for IHC) was obtained from Santa Cruz Biotechnology. Anti-HER2 antibody (#2156S; 1:100 diluted for IB and 1:100 diluted for IHC), anti-cleaved poly(adenosine 5′-diphosphate–ribose) polymerase ($Asp^{214}$) (#5625; 1:1000 diluted for IB), anti-cleaved caspase 3 ($Asp^{175}$) (#9664; 1:1000 diluted for IB), anti–phospho-MLKL (mixed lineage kinase domain like pseudokinase) ($Ser^{358}$) (#91689; 1:1000 diluted for IB), anti-HMGB1 (#6893; 1:1000 diluted for IB), anti-mouse CD8α (#70306; 1:200 diluted for IHC), and anti-PRF1 (#31647; 1:400 diluted for IHC) were purchased from Cell Signaling Technology. Anti-actin (sc-1616; 1:5000 diluted for IB), horseradish peroxidase (HRP)–anti-mouse IgG (sc-2055; 1:5000 diluted for IB), HRP-mouse IgGκ binding protein (sc-516102; 1:5000 diluted for IB), and HRP–anti-rabbit IgG (sc-2054; 1:5000 diluted for IB) were purchased from Santa Cruz Biotechnology. Anti–GZMB (ab237847; 1:100 diluted for IHC), anti-calreticulin antibody (ab196158; 1:100 diluted for flow cytometry), and isotype IgG (ab199091; 1:100 diluted for flow cytometry) were purchased from Abcam. Anti-IFNAR1 (clone MAR1–5A3; 10 μg/ml for blocking IFNAR1) and isotype-matched control antibodies (clone MOPC-211; 10 μg/ml) were purchased from Bio X Cell. Anti-HER2 antibody (#340552; 1:50 diluted for flow cytometry) was purchased from BD Biosciences. Anti–annexin V (#640906; 1:100 diluted for flow cytometry), anti-CD11c (#117312; 1:100 diluted for flow cytometry), anti-CD86 (#105015; 1:100 diluted for flow cytometry), anti-CD80 (#104705; 1:100 diluted for flow cytometry), anti–MHC-II (#107631; 1:100 diluted for flow cytometry), anti–CD3-phycoerythrin (PE)/Cy7 (clone 17A2; 1:100 diluted for flow cytometry), anti–CD4-AF700 (clone GK1.5; 1:100 diluted for flow cytometry), anti–CD8a-allophycocyanin (APC)/Cy7 (clone 53–6.7; 1:100 diluted for flow cytometry), anti–CD45-BV605 (clone 30-F11; 1:100 diluted for flow cytometry), anti–IFN-γ–BV786 (clone XMG1.2; 1:50 diluted for flow cytometry), anti–GZMB–PerCP/Cy5.5 (clone QA16A02; 1:50 diluted for flow cytometry), and mouse Fc block (#101302; 1:100 diluted for flow cytometry) were purchased from BioLegend. Human Fc receptor binding inhibitor antibody (#14–9161-73; 1:50 diluted for Fc blocking), goat anti-human antibody (#A-11014; 1:200 diluted for flow cytometry), control small interfering RNAs (siRNAs), and siRNAs against HMGB1 (s205520, s67572, and s67574) were purchased from Thermo Fisher Scientific.

## Genomic DNA isolation and copy number validation

Total genomic DNA was extracted either from cell lines using DNeasy Blood and Tissue Kit (QIAGEN) or from human tissue specimen using QIAamp DNA FFPE Tissue Kit (QIAGEN) according to the manufacturer's protocols. The copy number variations for

*PSMB6* (HS01025813_cn), *TP53* (Hs06423639_cn), *POLR2A* (Hs02023849), and *FLCN* (Hs00954797) were determined using TaqMan probes (Thermo Fisher Scientific) and the standard TaqMan PCR kit (no. A30866, Thermo Fisher Scientific). *TERT* (no. 4403316, Thermo Fisher Scientific) was quantified as the reference gene in the same reaction for each DNA sample analysis.

## Generation of 17p$^{loss}$ HS578T cells and 11B$^{loss}$ EO771 cells

A vector (#83480, Addgene) expressing Cas9 and single guide RNA (sgRNA) was digested with BsmBI and treated with AP, followed by 1% agarose gel purification of the linearized vector DNA. A pair of oligos for sgRNA targeting were annealed and phosphorylated. The sequences of oligo DNA are as follows: 5′-CAGCCGACTGAACAGCCGTA-3′ (WDR81), 5′-GAGGCAGACTCACGTGGGGT-3′ (MAP2K3), 5′-CTTCCGTGCAGAAGAGCGTG-3′ (FLCN), and 5′-CACTACATCATCAACAGCAG-3′ (CRK). The annealed oligos were subsequently ligated to linearized vectors. To generate 17p$^{loss}$ isogenic HS578T cells, the vectors expressing single guide RNA (sgRNA) targeting *WDR81* and *MAP2K3* were transduced into HS578T cells by electroporation. Similarly, to generate 11B loss isogenic EO771 cells, vectors expressing sgRNA targeting *Flcn* and *Crk* were transduced into EO771 cells. The resulting colonies were screened for large fragment deletion by PCR using primers 5′-GAGCCTGTCCTCACCTACCA-3′ and 5′-TGGCTGCTGAGCATCTACAC-3′ for generation of 17p loss in human cells and using primers 5′-CTCTTTGCA ATGACTGTTGGAG-3′ and 5′-CATTCTGAGTACCACTGCCAAA-3′ for 11B loss in murine cells. The heterozygous loss of 17p was validated by Sanger sequencing of the break point junction, copy number analysis of four genes (*PSMB6*, *TP53*, *POLR2A*, and *FLCN*) on the chromosome 17p by quantitative PCR, and protein expression analysis of POLR2A by IB. The heterozygous loss of 11B was also validated by Sanger sequencing of the break point junction and protein expression analysis of POLR2A by IB. To ectopically express POLR2A in 17p$^{loss}$ HS578T cells, *POLR2A* was PCR amplified with Flag-POLR2A vector (#35175, Addgene) as a template and was subsequently cloned into a pCDH-CMV lentiviral vector (#72265, Addgene). The resulting lentivirus was transduced to 17p$^{loss}$ HS578T cells.

## Flow cytometry

Cells were washed once with cold PBS and preincubated with human Fc receptor binding inhibitor antibody (for Fc blocking in human cells) or mouse CD16/CD32 (for Fc blocking in murine cells) that are diluted in flow cytometry staining buffer (PBS buffer containing 0.5% BSA) for 15 min at room temperature before staining. Cells were then washed once and incubated with the desired antibodies diluted in flow cytometry staining buffer for 40 min at 4°C. Cells were washed once and subjected to acquisition. For intracellular staining, after the cell surface staining, the cells were fixed and permeabilized using the Cytofix/Cytoperm fixation permeabilization kit (#554714, BD Biosciences). Cells were then incubated with the desired antibodies diluted in the Cytoperm buffer (#554714, BD Biosciences). Cells were washed once and subjected to acquisition. Acquisition was performed using an LSRFortessa X-20 or LSRFortessa (BD Biosciences). Flow data analysis was performed using FlowJo version 11.

### Determination of HER2 status in cell lines

The HER2 levels on the cell surface were characterized by quantitative fluorescence-activated cell sorting using an anti-HER2 antibody. To calculate the number of HER2 molecules per cell, Quantum Simply Cellular microspheres (#815, Bangs Laboratories) were stained with the same HER2 antibody, run in the same type of suspending solution/medium, on the same instrument, at the same instrument settings (photomultiplier tube voltages and compensation settings), and on the same day as cell samples. Median channel values were recorded, and a regression associating fluorescence channel value to the beads' ABC values is calculated. ABC values are assigned to stained cell samples based on the MFI of HER2 of the samples using this standard curve. The ABC value is equal to the number of HER2 surface receptors. To ectopically express HER2 in non-HER2–expressing cells, HS578T or EO771 cells were transduced with lentivirus encoding HER2 protein (Lvp504, Gentarget). Colonies were validated by flow cytometry and IB with the same method described in "Flow cytometry" section and "Immunoblotting" section.

### Cell survival assay

Cells with ~20% confluence were plated in 12-well plates in triplicate. After 24 hours, the cells were treated with trastuzumab, T-Ama, T-DM1, Crm, doxorubicin, and α-amanitin at indicated concentrations for 72 hours. Cells were subjected to 10% methanol fixation and 0.1% crystal violet staining (dissolved in 10% methanol). Wells were then washed three times and destained with acetic acid. The absorbance of the crystal violet solution was measured at 590 nm.

### Flow cytometry analysis of cell death

Cell death was analyzed using the FITC Annexin V Apoptosis Detection Kit I (#556547, BD Bioscience) following the manufacturer's instruction. Briefly, $1 \times 10^6$ cells were washed twice with cold PBS and resuspended in 1× binding buffer [0.1 M Hepes/NaOH (pH 7.4), 1.4 M NaCl, and 25 mM $CaCl_2$] containing FITC-conjugated annexin V and propidium iodide. Samples were then incubated for 15 min at room temperature in the dark and analyzed by flow cytometry. Pancaspase inhibitor Z-VAD(Ome)-FMK (#14463) and receptor interacting protein kinase 1 (RIPK1) kinase inhibitor necrostatin-1 (#11658) were purchased from Cayman Chemical.

### Immunohistochemistry

Breast tissue microarray or murine tumor sections were deparaffinized in xylene, rehydrated, and boiled for 10 min in antigen retrieval buffer [0.01 M sodium citrate buffer (pH 6.0)]. The sections were then washed with distilled water and incubated with 3% hydrogen peroxide for 10 min to block endogenous peroxidase activity. Next, the sections were blocked with 5% normal goat serum, followed by incubating with indicated primary antibodies at 4°C overnight. The samples were then washed with distilled water and incubated with secondary antibodies. A streptavidin-biotin peroxidase detection system was used to develop the signal according to the manufacturer's instructions [3,3′-Diaminobenzidine (DAB) peroxidase substrate kit, Vector Laboratories]. Counterstaining was carried out using Harris modified hematoxylin. All immunostained slides were scanned on the Automate Cellular Image

System III (Dako) for quantification by digital image analysis. The HER2 score was determined by independent pathological analysis.

## Immunoblotting

Cell lysates were prepared using cell lysis buffer [50 mM tris (pH 7.5), 150 mM NaCl, 1 mM EDTA, 0.5% NP-40, 0.5% Triton X-100, 1 mM phenylmethylsulfonyl fluoride, 1 mM sodium fluoride, 5 mM sodium vanadate, and aprotinin, leupeptin, and pepstatin (1 μg/ml)]. Proteins were then resolved by SDS–polyacrylamide gel electrophoresis and subsequently transferred to polyvinylidene difluoride membranes (Millipore). Membranes were then blocked with 5% milk, followed by incubation with indicated primary antibodies overnight. Membranes were then washed and incubated with peroxidase-conjugated secondary antibodies. Last, the relevant protein was visualized by enhanced chemiluminescence system (PerkinElmer) according to the manufacturer's instructions.

## RNA isolation and quantitative PCR

Total RNA was isolated using the RNeasy Mini Kit (QIAGEN) and then reverse-transcribed with the qScript cDNA (complementary DNA) Synthesis Kit (Quantabio). The resulting cDNA was used for quantitative PCR using the PerfeCTa SYBR Green Supermix (Quantabio) with gene-specific primers, and the results were normalized to PPIA (peptidylprolyl isomerase A) control. The primer sequences are as follows:

MX dynamin like GTPase 1 (MX1), 5′-GTTTCCGAAGTGGACATCGCA-3′ and 5′-CTGCACAGGTTGTTCTCAGC-3′; 2′−5′-oligoadenylate synthetase 2 (OAS2), 5′-ACGTGACATCCTCGATA AAACTG-3′ and 5′-GAACCCATCAAGGGACTTCTG-3′; radical S-adenosyl methionine domain containing 2 (RSAD2), 5′-TTGGACATTCTCGCTATCTCCT-3′ and 5′-AGTGCTTTGATCTGTTCCGTC-3′; C-C motif chemokine ligand 4 (CCL4), 5′-CTGTGCTGATCCCAGTGAATC-3′ and 5′-TCAGTTCAGTTCCAGGTCATACA-3′; tumor necrosis factor (TNF), 5′-GAGGCCAAGCCCTGGTATG-3′ and 5′-CGGGCCGATTGATCTCAGC-3′; interferon regulatory factor 1 (IRF1), 5′-CTGTGCGAGTGTACCGGATG-3′ and 5′-ATCCCCACATGACTTCCTCTT-3′; C-C motif chemokine ligand 2 (CCL2), 5′-CAGCCAGATGCAATCAATGCC-3′ and 5′-TGGAATCCTGAACCCACTTCT-3′; C-X-C motif chemokine ligand 1 (CXCL1), 5′-AAC-CGAAGTCATAGCCACAC-3′ and 5′-GTTGGATTTGTCACT GTTCAGC-3′; C-X-C motif chemokine ligand 10 (CXCL10), 5′-GTGGCATTCAAGGAGTACCTC-3′ and 5′-TGATGGCCTTCGATTCTGGATT-3′; interferon beta 1 (IFNB1), 5′-ATGACCAACAAGTGTCTCCTCC-3′ and 5′-GGAATCCAAGCAAGTTGTAGCTC-3′; peptidylprolyl isomerase A (PPIA), 5′-AGGTCCCAAAGACAGCAGAA-3′ and 5′-GAAGTCACCACCCTGACACA-3′.

## Synthesis and characterization of T-Ama

The anti-HER2 α-amanitin ADC (T-Ama) is based on the sequence of trastuzumab (Herceptin, Roche). Trastuzumab was modified at position 265 to introduce a cysteine at this position for conjugation using the THIOMAB technology (47, 48). The resulting THIOMAB derivative of trastuzumab was generated using Expi293 cells (Life Technologies) and transient transfection methods. The engineered cysteine residues of

the anti-HER2 THIOMAB antibody were used for conjugation of the cysteine reactive linker–amanitin compound, HDP 30.1699, with a cleavable linker by maleimide chemistry. Briefly, the THIOMAB in PBS (pH 7.4) was reduced with tris(2-carboxyethyl)phosphine, and interchain disulfides were reoxidized by dehydro ascorbic acid. Subsequently, the engineered cysteines were used for conjugation with cysteine reactive linker–amanitin compound, HDP 30.1699. The drug-antibody ratio according to liquid chromatography–mass spectrometry analysis was two toxins per IgG. The conjugate was purified by size-exclusion fast protein liquid chromatography and dialysis.

### Enzyme-linked immunosorbent assay

Single cells from dissociated tumors were seeded in Dulbecco's modified Eagle's medium (#D6429, Sigma-Aldrich) culture medium supplemented with 10% FBS (35–011-CV, Corning) and 1% penicillin/streptomycin (SV30010, HyClone). Cells were incubated for 4 hours with phorbol myristate acetate (50 ng/ml) and ionomycin (750 ng/ml) to stimulate the secretion of cytokines. Media were collected and centrifuged to remove cells and debris after incubation. The levels of IFN-γ and TNFα in the supernatants were immediately detected using ELISA kits (ELISA MAX Deluxe Set Mouse IFN-γ, catalog no. 430804, BioLegend; and ELISA MAX Deluxe Set Mouse TNFα, catalog no. 430904, BioLegend) according to the manufacturer's instructions.

### BMDC maturation assay

Bone marrow was isolated from the femurs of C57BL/6J mice at the age of 7 to 10 weeks. Bone marrow was next induced to differentiate into BMDCs in RPMI-1640 medium (R8758, Sigma-Aldrich) supplemented with 5% heat-inactivated FBS (35–011-CV, Corning), mouse granulocyte-macrophage colony-stimulating factor (GM-CSF) (20 ng/ml) (#315–03, PeproTech). Fresh medium containing mGM-CSF (20 ng/ml) was added on days 2, 4, and 6. The percentage of BDMCs was measured by flow cytometry. Immature murine BMDCs were coincubated with dying EO771 cells stimulated with Crm, doxorubicin, and α-amanitin as indicated for 18 hours. As a positive control, BMDCs were stimulated in parallel with *Escherichia coli* LPS (100 ng/ml). After coincubation, the cells were collected, centrifuged (400*g* for 6 min at 4°C), and washed once in PBS. Dead cells were excluded from the flow cytometry analysis by staining with SYTOX Blue (S11348, Molecular Probes). Maturation of BMDCs was analyzed by immunostaining with anti-CD11c, anti-CD86, anti-CD80, anti–MHC-II, and mouse Fc block. Meanwhile, the supernatants were also collected to check the cytokine secretion from BMDCs. The ELISA kits used here include TNFα ELISA (#430904, BioLegend), IL-6 (#431304, BioLegend), IL-12p70 (#433604, BioLegend), IL-1β (#432604, BioLegend), IL-10 (#431414, BioLegend), and TGFβ1 (#437707, BioLegend).

### Mass cytometry

Single-cell suspensions from EO771 tumors under different treatment conditions were prepared using a mouse tumor dissociation kit (Miltenyi Biotec) per the manufacturer's instructions. Tumor single cells were washed twice using fresh CyTOF buffer (ice-cold PBS containing 0.5% BSA and 0.02% sodium azide). To determine immune cell profiling, $1.5 \times 10^6$ live cells were used for each sample to be stained with the antibody panel 1

(table S1). To determine T cell activity, $1.5 \times 10^6$ live cells were stained with antibodies included in the panel 2 for T cell analysis (table S2). CyTOF data were analyzed with viSNE algorithm from Cytobank platform with 7500 iterations, 30 perplexity, and 0.5 thera (49). We next performed SPADE (Spanning-tree Progression Analysis of Density-normalized Events) analysis based on the viSNE analysis. The cell population was then gated manually on the SPADE TREE based on the selected markers and visualized on viSNE as an overlaid plot.

### Breast tumor xenograft mouse model

Female Nu/J mice were purchased from the Jackson laboratory. BT20 ($5 \times 10^6$) or HCC70 ($1 \times 10^6$) cancer cells in 100 μl of PBS with 50% Matrigel (BD Biosciences) were injected orthotopically into the fourth mammary gland of 5- to 6-week-old female mice. Once the tumors reached a palpable size (50 to 75 $mm^3$), the animals were randomized to four groups ($n = 8$ per group): (i) trastuzumab, 20 mg/kg; (ii) T-Ama, 2.0 mg/kg; (iii) T-Ama, 0.5 mg/kg; and (iv) T-Ama, 0.1 mg/kg. The treatment was administrated on days 12 and 19. Similarly, in the mice bearing tumors derived from HER2-low/17p$^{intact}$ ($2 \times 10^6$) or HER2-low/17p$^{loss}$ HS578T ($2 \times 10^6$) cancer cells, the mice were randomized to four groups ($n = 8$ per group): (i) trastuzumab, 20 mg/kg; (ii) T-DM1, 2.0 mg/kg; (iii) T-Ama, 2.0 mg/kg; and (iv) T-Ama, 0.5 mg/kg. The treatment was given on days 12 and 19. Tumor growth was recorded using digital calipers, and tumor volumes were calculated using the formula $0.5 \times L \times W^2$, where $L$ is the longest diameter and $W$ is the shortest diameter. The mice were euthanized when they become moribund or the tumor volume reached 1000 $mm^3$. The overall survival curve of mice was plotted by Kaplan-Meier survival analysis. Mouse body weight during the course of the study was monitored every other day. When mice were euthanized, tumors were extracted and processed for sectioning and IHC staining.

### PDX mouse model

The PDX studies were performed by XenTech as a customized service. The PDX models were established without prior in vitro culture and have been studied for histology, cytogenetics, genetic and other biological markers and for their response to standard-of-care therapies. The HBCx-10 PDX model is a TNBC with mutated *TP53* and *BRCA2*, 17p$^{intact}$, and low HER2 overexpression (IHC 1+). The HBCx-11 PDX model was obtained from a primary TNBC with mutated *TP53*, 17p$^{loss}$, and low HER2 overexpression (IHC 1+). The HBCx-11 PDX tumor was not responsive to cetuximab and trastuzumab. Outbred athymic (nu/nu) female mice weighing 18 to 25 g (ENVIGO) were used for this study. Tumors of the same passage were transplanted subcutaneously onto four to eight mice. When these tumors reached 936 to 1913 $mm^3$, donor mice were euthanized. Tumors were aseptically excised and cut into ~20-$mm^3$ fragments and transferred subcutaneously into the subsequent passage mice. Once the tumor reached a mean volume of ~150 $mm^3$, 10 mice per group were randomly allocated for treatment. Single intravenous treatment was administered 33 days (HBCx-10) after tumor implantation or 36 days (HBCx-11) after tumor implantation, respectively. Tumor volume was evaluated biweekly during the experimental period.

### In vivo tumor vaccination assay

Cell death was induced in EO771 by α-amanitin or EO771 (11B3$^{loss}$, HER2 1+) cells by T-Ama treatment as indicated. Next, the cells were collected, washed once in PBS, and resuspended at the desired cell density in PBS. C57BL/6 or C57BL/6-Tg(WapHER2) mice were inoculated subcutaneously with the α-amanitin– or T-Ama–treated cells ($5 \times 10^5$), respectively, on the left flank. Ten days after vaccination, the mice were rechallenged subcutaneously on the opposite flank with the corresponding EO771 cells or EO771 (11B3$^{loss}$, HER2 1+) cells ($5 \times 10^5$). Tumor growth at the challenge site was monitored for up to 100 days after the challenge. Mice were euthanized when the mice become moribund or the tumor exceeded 1000 $cm^3$.

### Syngeneic mouse model of breast cancer

Female C57BL/6-Tg(WapHER2) mice expressing human HER2 were obtained from the Jackson laboratory (stock no. 010562). HER2-low 11B$^{loss}$ EO771 cancer cells ($1 \times 10^6$) were implanted orthotopically into the fourth mammary gland of 6- to 8-week-old female transgenic mice. Once the tumors reached a palpable size (75 to 100 $mm^3$), the animals were randomized to four groups ($n = 10$ per group) for treatments: (i) trastuzumab, 20 mg/kg on days 7 and 14; (ii) T-Ama, 5.0 mg/kg on days 7 and 14; (iii) anti-mouse PD-1, 10 mg/kg on days 5, 7, 9, 12, and 14; and (iv) combo treatment, T-Ama (5.0 mg/kg on days 7 and 14) and PD-1 (10 mg/kg on days 5, 8, 10, 13, and 15). For T cell depletion, anti-CD4 (10 mg/kg) (GK1.5, rat IgG2b, Bio X Cell) and anti-CD8 (10 mg/kg) (53–6.72, rat IgG2a, Bio X Cell) were given at days −2 and 0 and then twice weekly until the end of the experiment. Tumor growth was recorded by tumor volumes. The mice were euthanized when they become moribund or the size of the tumor reaches 1000 $mm^3$.

### Tolerability study of T-Ama in nonhuman primates

A group of three cynomolgus monkeys was used for the tolerability study. The studies were performed in treatment-naive female cynomolgus monkeys at the Laboratory of Pharmacology and Toxicology GmbH and Co. KG. The animals (age 2 to 5 years, 2.6 to 3.1 kg of bodyweight at first dosing) were kept according to German animal protection law requirements. Female animals were chosen for this study concerning breast cancer with no prejudice to exclude males. Animals received a nonbinding control antibody (anti-digoxigenin) conjugated to α-amanitin intravenously (slow bolus) in escalating doses (0.3, 1, and 3 mg/kg; doses), and serum was obtained at indicated time points. Animals were monitored over time for biochemical and hematological blood parameters, body weight, food consumption, clinical signs, and mortality.

### Statistical analysis

Statistical analysis was conducted using GraphPad Prism 7 and R. Differences between two groups were tested with unpaired twotailed Student's *t* tests. A one-way analysis of variance (ANOVA) followed by Tukey's *t* test or two-way ANOVA where indicated was conducted to compare three or more groups of independent samples for normally distributed data. Time-dependent comparisons were tested using a two-way ANOVA with Tukey's test for correction. Kaplan-Meier plots were used for survival curves and analyzed with a log-rank

test. The results are displayed as the means ± SD. The level of significance was shown by asterisks: *$P < 0.05$, **$P < 0.01$, ***$P < 0.001$, and ****$P < 0.0001$. n.s. indicates not significant.

## Supplementary Material

Refer to Web version on PubMed Central for supplementary material.

## Acknowledgments:

We thank H. Broxmeyer, C. Zhang, B. Zhou, and K. Huang for insightful suggestions. We thank the Lu lab and Zhang lab members for technical support. We thank J. Wang at Baylor College of Medicine for help on chemical biology assays. We thank A. Colter for help on tissue microarray analysis. We are grateful for the technical services provided by Indiana University Histology Core and Flow Cytometry Resource Facility.

**Funding:**

This work was supported in part by U.S. NIH grants R01CA203737 (to X.L.), R01CA211861 (to B.H.), and R21CA213535 (to X.L.) and by Indiana University Strategic Research Initiative fund (to X.L.) and Vera Bradley Foundation for Breast Cancer Research (to X.L. and X.Z.).

## REFERENCES AND NOTES

1. Chen LC, Neubauer A, Kurisu W, Waldman FM, Ljung BM, Goodson III W, Goldman ES, Moore II D, Balazs M, Liu E., Loss of heterozygosity on the short arm of chromosome 17 is associated with high proliferative capacity and DNA aneuploidy in primary human breast cancer. Proc. Natl. Acad. Sci. U.S.A 88, 3847–3851 (1991). [PubMed: 1673792]
2. Li Y, Liu Y, Xu H, Jiang G, Van der Jeught K, Fang Y, Zhou Z, Zhang L, Frieden M, Wang L, Luo Z, Radovich M, Schneider BP, Deng Y, Liu Y, Huang K, He B, Wang J, He X, Zhang X, Ji G, Lu X., Heterozygous deletion of chromosome 17p renders prostate cancer vulnerable to inhibition of RNA polymerase II. Nat. Commun 9, 4394 (2018). [PubMed: 30349055]
3. Liu Y, Zhang X, Han C, Wan G, Huang X, Ivan C, Jiang D, Rodriguez-Aguayo C, Lopez-Berestein G, Rao PH, Maru DM, Pahl A, He X, Sood AK, Ellis LM, Anderl J, Lu X., TP53 loss creates therapeutic vulnerability in colorectal cancer. Nature 520, 697–701 (2015). [PubMed: 25901683]
4. Scarpa A, Di Pace C, Talamini G, Falconi M, Lemoine NR, Iacono C, Achille A, Baron A, Zamboni G., Cancer of the ampulla of Vater: Chromosome 17p allelic loss is associated with poor prognosis. Gut 46, 842–848 (2000). [PubMed: 10807898]
5. Menendez D, Inga A, Resnick MA, The expanding universe of p53 targets. Nat. Rev. Cancer 9, 724–737 (2009). [PubMed: 19776742]
6. Liu Y, Chen C, Xu Z, Scuoppo C, Rillahan CD, Gao J, Spitzer B, Bosbach B, Kastenhuber ER, Baslan T, Ackermann S, Cheng L, Wang Q, Niu T, Schultz N, Levine RL, Mills AA, Lowe SW, Deletions linked to TP53 loss drive cancer through p53-independent mechanisms. Nature 531, 471–475 (2016). [PubMed: 26982726]
7. Xu J, Liu Y, Li Y, Wang H, Stewart S, Van der Jeught K, Agarwal P, Zhang Y, Liu S, Zhao G, Wan J, Lu X, He X., Precise targeting of POLR2A as a therapeutic strategy for human triple negative breast cancer. Nat. Nanotechnol. 14, 388–397 (2019). [PubMed: 30804480]
8. Levine AJ, Oren M., The first 30 years of p53: Growing ever more complex. Nat. Rev. Cancer 9, 749–758 (2009). [PubMed: 19776744]
9. Paik S, Hazan R, Fisher ER, Sass RE, Fisher B, Redmond C, Schlessinger J, Lippman ME, King CR, Pathologic findings from the National Surgical Adjuvant Breast and Bowel Project: Prognostic significance of erbB-2 protein overexpression in primary breast cancer. J. Clin. Oncol 8, 103–112 (1990). [PubMed: 1967301]
10. Slamon DJ, Clark GM, Wong SG, Levin WJ, Ullrich A, McGuire WL, Human breast cancer: Correlation of relapse and survival with amplification of the HER-2/neu oncogene. Science 235, 177–182 (1987). [PubMed: 3798106]

11. Thor AD, Liu S, Edgerton S, Moore II D, Kasowitz KM, Benz CC, Stern DF, DiGiovanna MP, Activation (tyrosine phosphorylation) of ErbB-2 (HER-2/neu): A study of incidence and correlation with outcome in breast cancer. J. Clin. Oncol 18, 3230–3239 (2000). [PubMed: 10986055]
12. Wolff AC, Hammond ME, Schwartz JN, Hagerty KL, Allred DC, Cote RJ, Dowsett M, Fitzgibbons PL, Hanna WM, Langer A, McShane LM, Paik S, Pegram MD, Perez EA, Press MF, Rhodes A, Sturgeon C, Taube SE, Tubbs R, Vance GH, van de Vijver M, Wheeler TM, Hayes DF; American Society of Clinical Oncology/College of American Pathologists, American Society of Clinical Oncology/College of American Pathologists guideline recommendations for human epidermal growth factor receptor 2 testing in breast cancer. J. Clin. Oncol 25, 118–145 (2007). [PubMed: 17159189]
13. Romond EH, Perez EA, Bryant J, Suman VJ, Geyer CE Jr., Davidson NE, Tan-Chiu E, Martino S, Paik S, Kaufman PA, Swain SM, Pisansky TM, Fehrenbacher L, Kutteh LA, Vogel VG, Visscher DW, Yothers G, Jenkins RB, Brown AM, Dakhil SR, Mamounas EP, Lingle WL, Klein PM, Ingle JN, Wolmark N., Trastuzumab plus adjuvant chemotherapy for operable HER2-positive breast cancer. N. Engl. J. Med 353, 1673–1684 (2005). [PubMed: 16236738]
14. Dieras V, Miles D, Verma S, Pegram M, Welslau M, Baselga J, Krop IE, Blackwell K, Hoersch S, Xu J, Green M, Gianni L., Trastuzumab emtansine versus capecitabine plus lapatinib in patients with previously treated HER2-positive advanced breast cancer (EMILIA): A descriptive analysis of final overall survival results from a randomised, open-label, phase 3 trial. Lancet Oncol 18, 732–742 (2017). [PubMed: 28526536]
15. Fehrenbacher L, Cecchini RS, Geyer CE Jr., Rastogi P, Costantino JP, Atkins JN, Crown JP, Polikoff J, Boileau JF, Provencher L, Stokoe C, Moore TD, Robidoux A, Flynn PJ, Borges VF, Albain KS, Swain SM, Paik S, Mamounas EP, Wolmark N., NSABP B-47/NRG oncology phase III randomized trial comparing adjuvant chemotherapy with or without trastuzumab in high-risk invasive breast cancer negative for HER2 by FISH and with IHC 1+ or 2. J. Clin. Oncol 38, 444–453 (2020). [PubMed: 31821109]
16. Modi S, Park H, Murthy RK, Iwata H, Tamura K, Tsurutani J, Moreno-Aspitia A, Doi T, Sagara Y, Redfern C, Krop IE, Lee C, Fujisaki Y, Sugihara M, Zhang L, Shahidi J, Takahashi S., Antitumor activity and safety of trastuzumab deruxtecan in patients With HER2-low-expressing advanced breast cancer: Results from a phase Ib study. J. Clin. Oncol 38, 1887–1896 (2020). [PubMed: 32058843]
17. Chang WN, Wan CL, Sun YF, Han Y, Qi SY, Lu XB, Cao S, Zhang C., Abstract 2439: A semi-supervised deconvolution method for quantifying the composition and activity of tumor-infiltrating cell types. Cancer Res 79, 2439 (2019).
18. Chen B, Khodadoust MS, Liu CL, Newman AM, Alizadeh AA, Profiling tumor infiltrating immune cells with CIBERSORT. Methods Mol. Biol 1711, 243–259 (2018). [PubMed: 29344893]
19. Enjalbert F, Rapior S, Nouguier-Soule J, Guillon S, Amouroux N, Cabot C., Treatment of amatoxin poisoning: 20-year retrospective analysis. J. Toxicol. Clin. Toxicol 40, 715–757 (2002). [PubMed: 12475187]
20. Letschert K, Faulstich H, Keller D, Keppler D., Molecular characterization and inhibition of amanitin uptake into human hepatocytes. Toxicol. Sci 91, 140–149 (2006). [PubMed: 16495352]
21. Hendriks BS, Klinz SG, Reynolds JG, Espelin CW, Gaddy DF, Wickham TJ, Impact of tumor HER2/ERBB2 expression level on HER2-targeted liposomal doxorubicin-mediated drug delivery: Multiple low-affinity interactions lead to a threshold effect. Mol. Cancer Ther 12, 1816–1828 (2013). [PubMed: 23723124]
22. Cong L, Ran FA, Cox D, Lin SL, Barretto R, Habib N, Hsu PD, Wu XB, Jiang WY, Marraffini LA, Zhang F., Multiplex genome engineering using CRISPR/Cas systems. Science 339, 819–823 (2013). [PubMed: 23287718]
23. Mali P, Yang LH, Esvelt KM, Aach J, Guell M, DiCarlo JE, Norville JE, Church GM, RNA-guided human genome engineering via Cas9. Science 339, 823–826 (2013). [PubMed: 23287722]
24. Rodrigues DF, Pires das Neves R, Carvalho ATP, Lourdes Bastos M, Costa VM, Carvalho F., In vitro mechanistic studies on α-amanitin and its putative antidotes. Arch. Toxicol 94, 2061–2078 (2020). [PubMed: 32193566]

25. Galluzzi L, Buque A, Kepp O, Zitvogel L, Kroemer G., Immunogenic cell death in cancer and infectious disease. Nat. Rev. Immunol 17, 97–111 (2017). [PubMed: 27748397]
26. Casares N, Pequignot MO, Tesniere A, Ghiringhelli F, Roux S, Chaput N, Schmitt E, Hamai A, Hervas-Stubbs S, Obeid M, Coutant F, Metivier D, Pichard E, Aucouturier P, Pierron G, Garrido C, Zitvogel L, Kroemer G., Caspase-dependent immunogenicity of doxorubicin-induced tumor cell death. J. Exp. Med 202, 1691–1701 (2005). [PubMed: 16365148]
27. Obeid M, Tesniere A, Ghiringhelli F, Fimia GM, Apetoh L, Perfettini JL, Castedo M, Mignot G, Panaretakis T, Casares N, Metivier D, Larochette N, van Endert P, Ciccosanti F, Piacentini M, Zitvogel L, Kroemer G., Calreticulin exposure dictates the immunogenicity of cancer cell death. Nat. Med 13, 54–61 (2007). [PubMed: 17187072]
28. Galluzzi L, Humeau J, Buque A, Zitvogel L, Kroemer G., Immunostimulation with chemotherapy in the era of immune checkpoint inhibitors. Nat. Rev. Clin. Oncol 17, 725–741 (2020). [PubMed: 32760014]
29. Vacchelli E, Sistigu A, Yamazaki T, Vitale I, Zitvogel L, Kroemer G., Autocrine signaling of type 1 interferons in successful anticancer chemotherapy. Onco. Targets. Ther 4, e988042 (2015).
30. Sistigu A, Yamazaki T, Vacchelli E, Chaba K, Enot DP, Adam J, Vitale I, Goubar A, Baracco EE, Remédios C, Fend L, Hannani D, Aymeric L, Ma Y, Niso-Santano M, Kepp O, Schultze JL, Tüting T, Belardelli F, Bracci L, Sorsa VL, Ziccheddu G, Sestili P, Urbani F, Delorenzi M, Lacroix-Triki M, Quidville V, Conforti R, Spano J-P, Pusztai L, Poirier-Colame V, Delaloge S, Penault-Llorca F, Ladoire S, Arnould L, Cyrta J, Dessoliers M-C, Eggermont A, Bianchi ME, Pittet M, Engblom C, Pfirschke C, Préville X, Uzè G, Schreiber RD, Chow MT, Smyth MJ, Proietti E, André F, Kroemer G, Zitvogel L., Cancer cell-autonomous contribution of type I interferon signaling to the efficacy of chemotherapy. Nat. Med 20, 1301–1309 (2014). [PubMed: 25344738]
31. Garg AD, Vandenberk L, Fang S, Fasche T, Van Eygen S, Maes J, Van Woensel M, Koks C, Vanthillo N, Graf N, de Witte P, Van Gool S, Salven P, Agostinis P., Pathogen response-like recruitment and activation of neutrophils by sterile immunogenic dying cells drives neutrophil-mediated residual cell killing. Cell Death Differ 24, 832–843 (2017). [PubMed: 28234357]
32. Aaes TL, Kaczmarek A, Delvaeye T, De Craene B, De Koker S, Heyndrickx L, Delrue I, Taminau J, Wiernicki B, De Groote P, Garg AD, Leybaert L, Grooten J, Bertrand MJ, Agostinis P, Berx G, Declercq W, Vandenabeele P, Krysko DV, Vaccination with necroptotic cancer cells induces efficient anti-tumor immunity. Cell Rep 15, 274–287 (2016). [PubMed: 27050509]
33. Kroemer G, Galluzzi L, Kepp O, Zitvogel L., Immunogenic cell death in cancer therapy. Annu. Rev. Immunol 31, 51–72 (2013). [PubMed: 23157435]
34. Piechocki MP, Ho YS, Pilon S, Wei WZ, Human ErbB-2 (Her-2) transgenic mice: A model system for testing Her-2 based vaccines. J. Immunol 171, 5787–5794 (2003). [PubMed: 14634087]
35. Carver EA, Stubbs L., Zooming in on the human-mouse comparative map: Genome conservation re-examined on a high-resolution scale. Genome Res 7, 1123–1137 (1997). [PubMed: 9414318]
36. Schmid P, Adams S, Rugo HS, Schneeweiss A, Barrios CH, Iwata H, Dieras V, Hegg R, Im SA, Shaw Wright G, Henschel V, Molinero L, Chui SY, Funke R, Husain A, Winer EP, Loi S, Emens LA; IMpassion130 Trial Investigators, Atezolizumab and nab-paclitaxel in advanced triple-negative breast cancer. N. Engl. J. Med 379, 2108–2121 (2018). [PubMed: 30345906]
37. D'Abreo N, Adams S., Immune-checkpoint inhibition for metastatic triple-negative breast cancer: Safety first? Nat. Rev. Clin. Oncol 16, 399–400 (2019). [PubMed: 31053774]
38. Page DB, Bear H, Prabhakaran S, Gatti-Mays ME, Thomas A, Cobain E, McArthur H, Balko JM, Gameiro SR, Nanda R, Gulley JL, Kalinsky K, White J, Litton J, Chmura SJ, Polley MY, Vincent B, Cescon DW, Disis ML, Sparano JA, Mittendorf EA, Adams S., Two may be better than one: PD-1/PD-L1 blockade combination approaches in metastatic breast cancer. NPJ Breast Cancer 5, 34 (2019). [PubMed: 31602395]
39. Bardia A, Mayer IA, Diamond JR, Moroose RL, Isakoff SJ, Starodub AN, Shah NC, O'Shaughnessy J, Kalinsky K, Guarino M, Abramson V, Juric D, Tolaney SM, Berlin J, Messersmith WA, Ocean AJ, Wegener WA, Maliakal P, Sharkey RM, Govindan SV, Goldenberg DM, Vahdat LT, Efficacy and safety of anti-trop-2 antibody drug conjugate sacituzumab govitecan (IMMU-132) in heavily pretreated patients with metastatic triple-negative breast cancer. J. Clin. Oncol 35, 2141–2148 (2017). [PubMed: 28291390]

40. Mariani G, Fasolo A, De Benedictis E, Gianni L., Trastuzumab as adjuvant systemic therapy for HER2-positive breast cancer. Nat. Clin. Pract. Oncol 6, 93–104 (2009). [PubMed: 19107109]
41. Verma S, Miles D, Gianni L, Krop IE, Welslau M, Baselga J, Pegram M, Oh DY, Dieras V, Guardino E, Fang L, Lu MW, Olsen S, Blackwell K; EMILIA Study Group, Trastuzumab emtansine for HER2-positive advanced breast cancer. N. Engl. J. Med 367, 1783–1791 (2012). [PubMed: 23020162]
42. Beck A, Goetsch L, Dumontet C, Corvaia N., Strategies and challenges for the next generation of antibody-drug conjugates. Nat. Rev. Drug Discov 16, 315–337 (2017). [PubMed: 28303026]
43. Thomas A, Teicher BA, Hassan R., Antibody-drug conjugates for cancer therapy. Lancet Oncol 17, e254–e262 (2016). [PubMed: 27299281]
44. Moldenhauer G, Salnikov AV, Luttgau S, Herr I, Anderl J, Faulstich H., Therapeutic potential of amanitin-conjugated anti-epithelial cell adhesion molecule monoclonal antibody against pancreatic carcinoma. J. Natl. Cancer Inst 104, 622–634 (2012). [PubMed: 22457476]
45. Ritchie ME, Phipson B, Wu D, Hu Y, Law CW, Shi W, Smyth GK, *limma* powers differential expression analyses for RNA-sequencing and microarray studies. Nucleic Acids Res 43, e47 (2015). [PubMed: 25605792]
46. Krzywinski M, Schein J, Birol I, Connors J, Gascoyne R, Horsman D, Jones SJ, Marra MA, Circos: An information aesthetic for comparative genomics. Genome Res 19, 1639–1645 (2009). [PubMed: 19541911]
47. Junutula JR, Bhakta S, Raab H, Ervin KE, Eigenbrot C, Vandlen R, Scheller RH, Lowman HB, Rapid identification of reactive cysteine residues for site-specific labeling of antibody-Fabs. J. Immunol. Methods 332, 41–52 (2008). [PubMed: 18230399]
48. Junutula JR, Raab H, Clark S, Bhakta S, Leipold DD, Weir S, Chen Y, Simpson M, Tsai SP, Dennis MS, Lu Y, Meng YG, Ng C, Yang J, Lee CC, Duenas E, Gorrell J, Katta V, Kim A, McDorman K, Flagella K, Venook R, Ross S, Spencer SD, Lee Wong W, Lowman HB, Vandlen R, Sliwkowski MX, Scheller RH, Polakis P, Mallet W., Site-specific conjugation of a cytotoxic drug to an antibody improves the therapeutic index. Nat. Biotechnol 26, 925–932 (2008). [PubMed: 18641636]
49. Kotecha N, Krutzik PO, Irish JM, Web-based analysis and publication of flow cytometry experiments. Curr. Protoc. Cytom 53, 10.17.1–10.17.24 (2010).

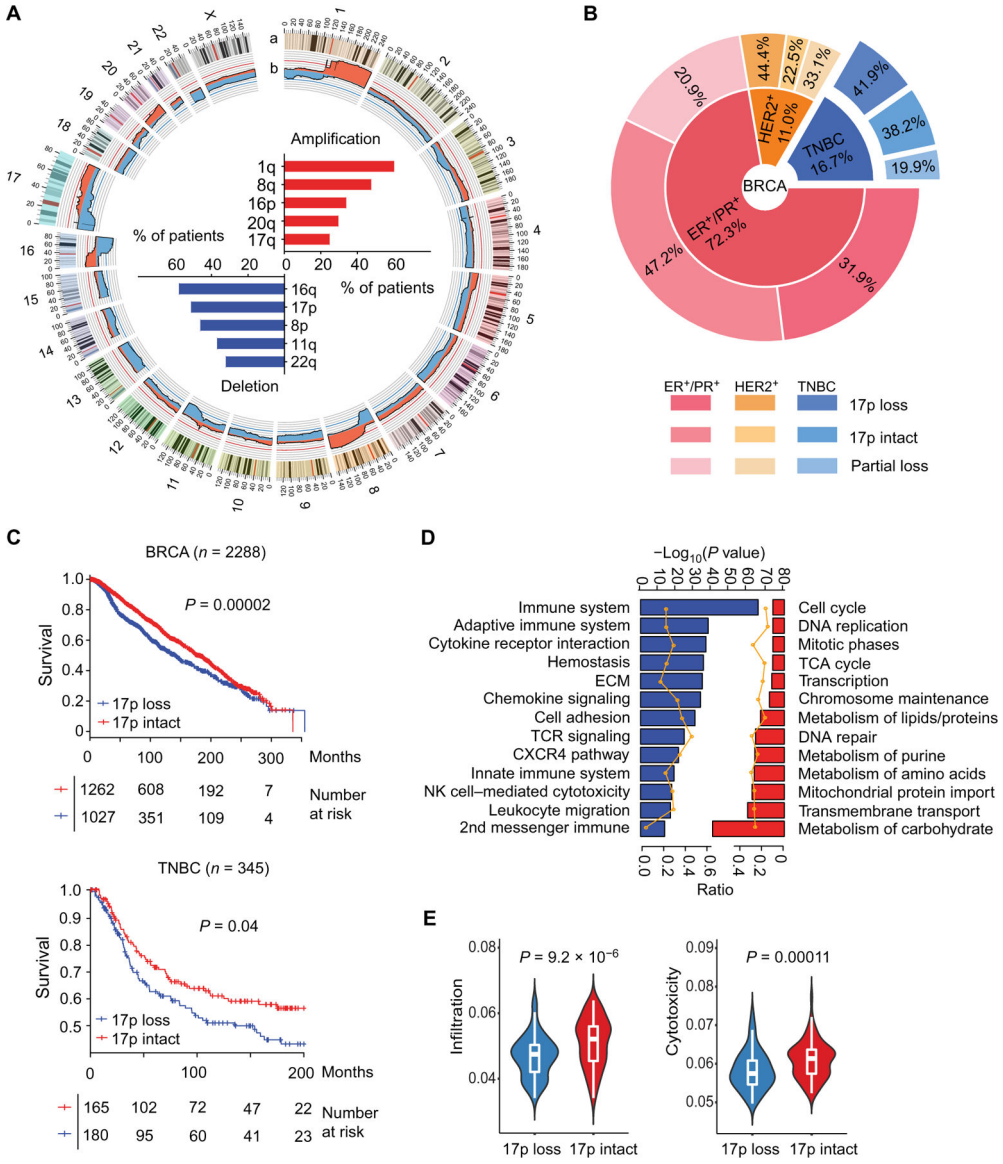


**Fig. 1. 17p$^{loss}$ is one of the most frequent chromosome abnormalities in breast cancer and correlates with low T cell infiltration and cytotoxicity in TNBC.**

(**A**) Circos plot depicts the distribution of various genomic attributes along the genetic map of human breast cancer (BRCA) from The Cancer Genome Atlas (TCGA) and Molecular Taxonomy of Breast Cancer International Consortium (METABRIC) cohorts, with tracks for chromosome ideograms and genome-wide copy number variation (red, amplification; blue, deletion). The center of the plot shows the percentage of patients with breast cancer with the most frequent chromosome amplification (red) or deletion (blue). (**B**) The proportions of breast cancer with various 17p statuses in each subtype are shown in the pie chart. The CNA data of 2590 patients with breast cancer from TCGA and the METABRIC cohorts were evaluated. (**C**) Kaplan-Meier survival curves of overall survival for patient groups with 17p$^{loss}$ or 17p$^{intact}$ using TCGA and METABRIC datasets. *P* values were determined by log-rank test. (**D**) The gene set enrichment analysis for 17p$^{loss}$ versus 17p$^{intact}$ TNBC (blue, down-regulated pathways; red, up-regulated pathways in 17p$^{loss}$ TNBC). The bar

chart represents significance of gene enrichment for any given pathway. The orange lines indicate the ratio or percent coverage of a pathway subject to pathway size bias. A *P* value of Fisher's exact test of <0.05 and a false discovery rate (FDR) of <0.01 were set as the cutoff criteria. ECM, extracellular matrix; TCA, tricarboxylic acid; TCR, T cell receptor; NK, natural killer. (**E**) Violin box plots showed the correlation of 17p status with infiltration and cytotoxicity of T cells in TNBC. The boxes represent the interquartile range (IQR). The line in the box represents the median. The lower edge line of the box represents the 25th percentile (Q1), whereas the upper edge line of the box represents the 75th percentile (Q3). The end point of the vertical line below the box represents the minimum value (Q1 − 1.5 * IQR), whereas the end point of the vertical line above the box represents the maximum value (Q3 + 1.5 * IQR). Data were analyzed with the ICTD algorithm on 251 patients with TNBC ($17p^{loss}$, 123 patients; $17p^{intact}$, 128 patients) from the METABRIC cohort.

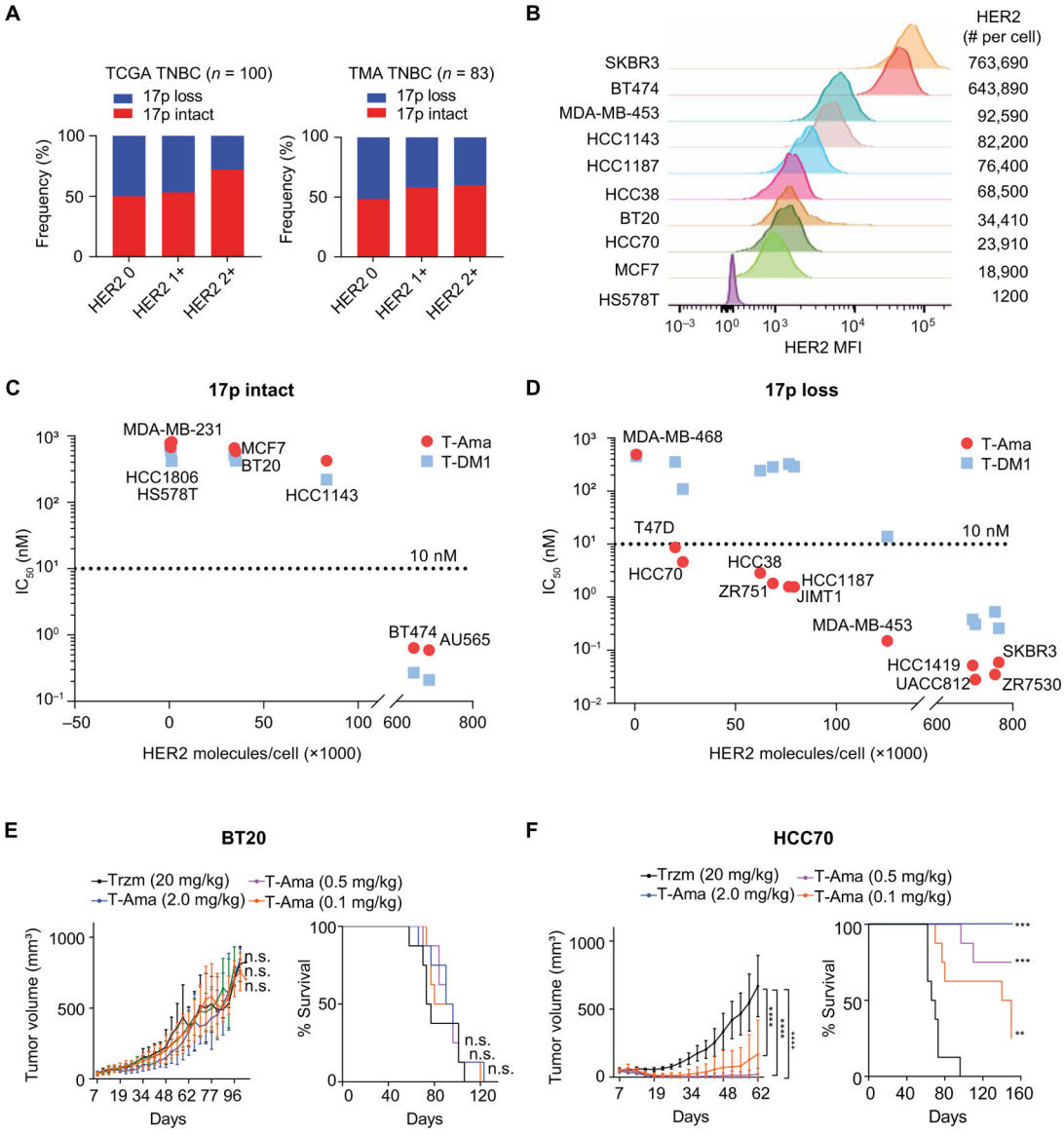


**Fig. 2. T-Ama exhibits superior efficacy in killing HER2-low TNBC cells with 17p$^{loss}$.**

(**A**) Frequencies of 17p$^{loss}$ and 17p$^{intact}$ in patients with TNBC with different HER2 scores from TCGA dataset or TNBC tissue microarrays (TMA). (**B**) The amounts of HER2 molecules on the surface of breast cancer cells were analyzed by flow cytometry. Median fluorescence intensity (MFI) of HER2 of standard microspheres with known antibody binding capacity (ABC) values was recorded. A regression curve associating fluorescence channel value to the beads' ABC is generated. ABC values are assigned to stained cell samples based on the MFI of HER2$^{+}$ populations of the cell samples using this standard curve. The value of ABC is equal to the number of HER2 molecules. $n = 3$. (**C** and **D**) The cytotoxicity of T-Ama (red dots) was compared to that of T-DM1 (blue squares) in terms of $IC_{50}$ value in indicated 17p$^{intact}$ (C) and 17p$^{loss}$ (D) breast cancer cell lines with different concentrations of HER2 on the cell surface. $IC_{50}$, half-maximal inhibitory concentration. $n = 3$. (**E** and **F**) Tumor growth curve and survival analysis in nude mice orthotopically

implanted with HER2-low 17p$^{intact}$ BT20 cells (E) and HER2-low 17p$^{loss}$ HCC70 cells (F). Mice were randomized to four groups ($n$ = 8 mice per group). On day 7 and day 14 after tumor inoculation, mice were intraperitoneally injected with either trastuzumab (Trzm) (20 mg/kg) or indicated doses of T-Ama. Data shown are means ± SD. Statistical analysis was conducted by two-way ANOVA with Tukey's test for correction for tumor burden among groups and by log-rank (Mantel-Cox) test for animal survival. n.s., not significant. ** $P$ < 0.01, *** $P$ < 0.001, and **** $P$ < 0.0001.

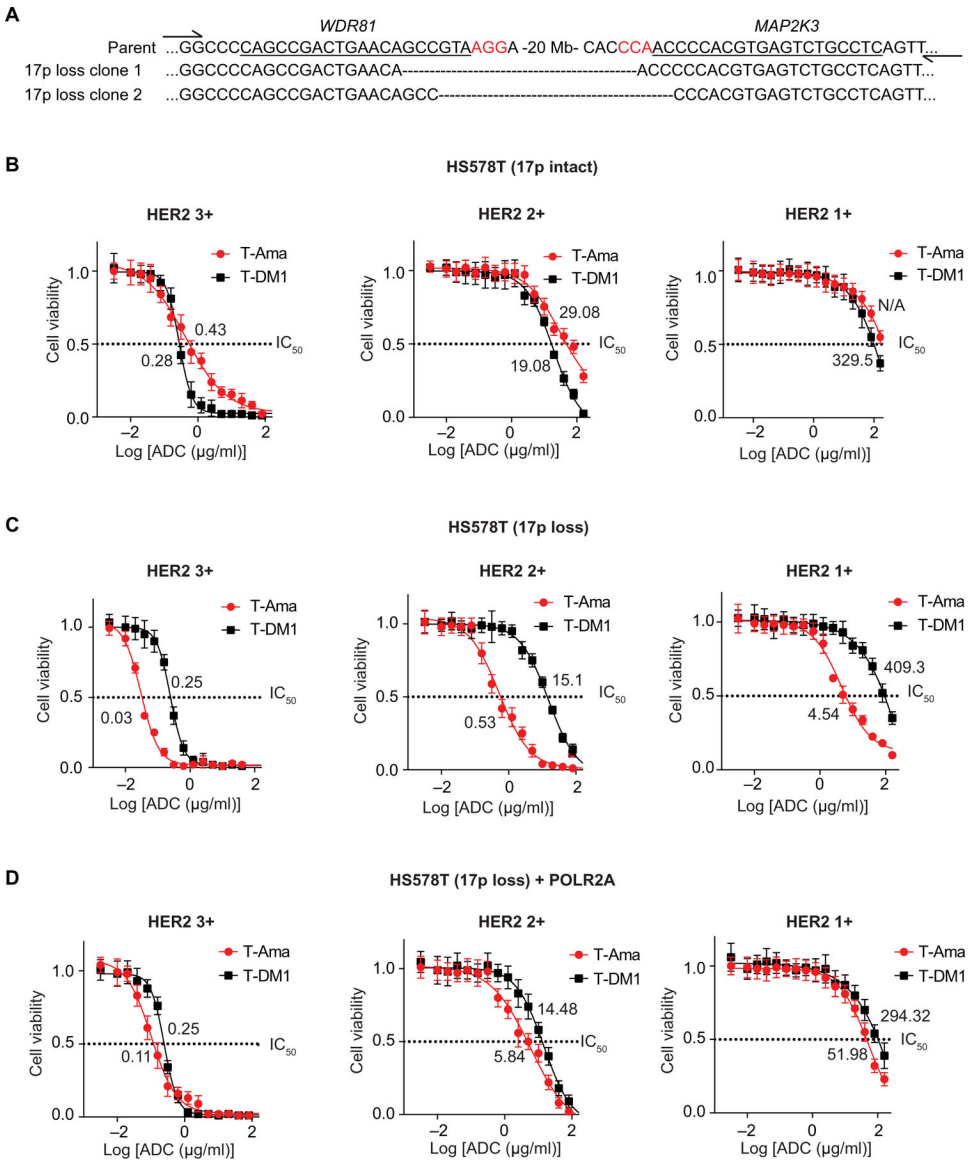


**Fig. 3. 17p loss renders HER2-low breast cancer cells highly vulnerable to T-Ama.**

(**A**) Generation of 17p deletion (~20 Mb) in HS578T cells using Cas9 and two sgRNAs (sgWDR81 and sgMAP2K3). The sgRNA-targeting sites were underlined, and the protospacer adjacent motif sequence was highlighted in red. Colonies were screened using primers flanking the residual *WDR81* and *MAP2K3* (indicated by the arrows). Sanger sequencing results confirmed the break point junction with the deletion region indicated by the dashes. (**B** and **C**) $17p^{intact}$ (B) and $17p^{loss}$ (C) HS578T cells with different HER2 levels (scores 1, 2, and 3) were treated in vitro with T-Ama and T-DM1. The $IC_{50}$ value is shown beside the curve. (**D**) Ectopic expression of POLR2A partially restored the resistance of $17p^{loss}$ HS578T cells to T-Ama. $IC_{50}$, half maximal inhibitory concentration; ADC, antibody-drug conjugate. The cell viability data were presented as means ± SD of three independent experiments ($N = 3$).

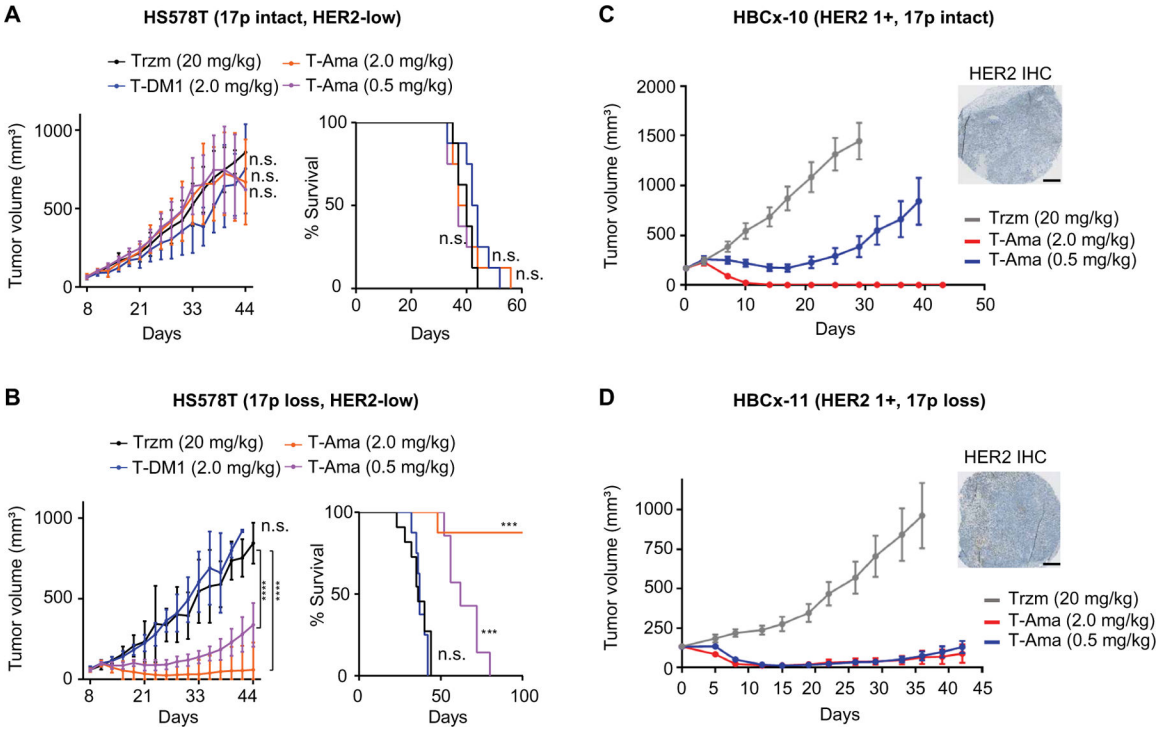


**Fig. 4. T-Ama exhibits in vivo antitumor activity in treating HER2-low breast cancer with 17p loss.**

(**A** and **B**) Tumor growth curve and survival analysis of nude mice orthotopically implanted with HER2-low $17p^{intact}$ (A) and the isogenic $17p^{loss}$ HS578T cells (B). Mice were randomized to four groups ($n$ = 8 mice per group) after tumors were established. On days 11 and 18 after tumor inoculation, mice were intraperitoneally injected with trastuzumab (Trzm), T-DM1, or T-Ama at indicated doses. Data shown are mean tumor volumes ± SD. (**C** and **D**) Tumor growth analysis of T-DM1–resistant HER2-low patient-derived xenograft with $17p^{intact}$ (C) or $17p^{loss}$ (D) in athymic (nu/nu) female mice. Tumors were intraperitoneally administered with a single dose of Trzm or T-Ama 33 days (HBCx-10) after tumor implantation or 36 days (HBCx-11) after tumor implantation. $n$ = 4 to 8 mice per group. Data shown are mean tumor volumes ± SD. Immunohistochemical staining of HER2 was shown for both tumor models. Scale bars, 0.3 mm. Statistical analysis was conducted by two-way ANOVA test with Tukey's test for correction for tumor burden among groups and by log-rank (Mantel-Cox) test for animal survival. n.s., not significant. ***$P < 0.001$ and ****$P < 0.0001$.

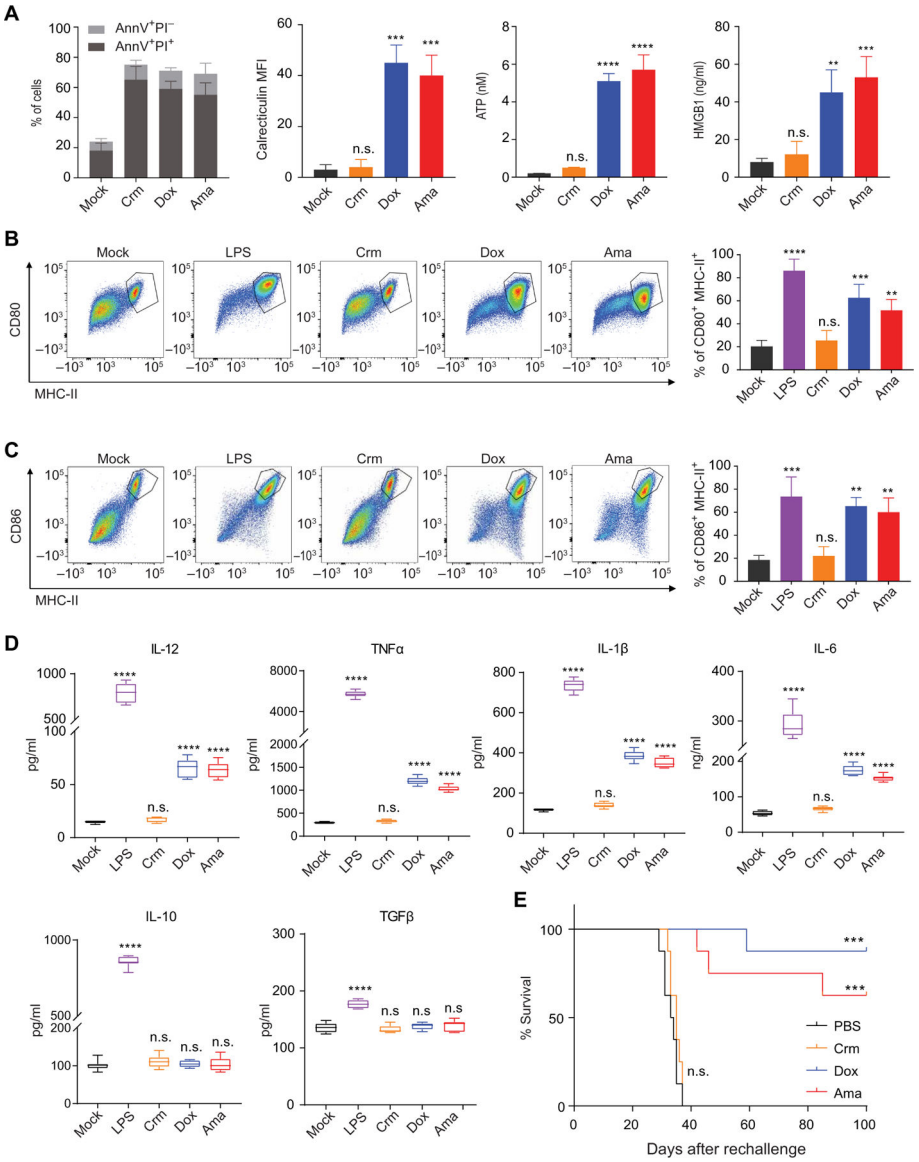


**Fig. 5. Treatment with α-amanitin induces immunogenic cell death in breast cancer cells.**

(**A**) Treatment with α-amanitin triggered calreticulin exposure on the cell surface and extracellular release of ATP and HMGB1 in MDA-MB-453 cells in vitro. MDA-MB-453 cells were treated with $IC_{50}$ dose of Crm (C2 ceramide), Dox (doxorubicin), or Ama (α-amanitin) for 72 hours, followed by assessment of the proportion of pre-apoptotic cells ($AnnV^+$, $PI^-$) and apoptotic cells ($AnnV^+$, $PI^+$). The MFI of calreticulin on the cell membrane was quantified on $PI^-$ cells. Extracellular ATP was measured with the ENLITEN ATP Assay System, whereas HMGB1 were detected with HMGB1 ELISA kit. AnnV, annexin V; PI, propidium iodide. All bars were compared to the mock bar. Statistical analysis was conducted by one-way ANOVA with Turkey's test for correction. $N = 3$ repeats. (**B** and **C**) Analysis of bone marrow–derived dendritic cell (BMDC) maturation induced by coculture with the cytotoxicant-treated EO771 cells. BMDCs were stimulated with lipopolysaccharide (LPS) or EO771 cells pretreated with Crm, Dox (doxorubicin), or

Ama (α-amanitin) for 72 hours. BMDC maturation was measured by MHC-II and CD80 expression (B) or MHC-II and CD86 expression (C) by flow cytometry. All bars were compared to the mock bar. Statistical analysis was conducted by one-way ANOVA with Turkey's test for correction. $N = 3$ repeats. (**D**) The cytokines in the supernatant of BMDCs were analyzed by ELISA. Tumor cells were pretreated with mock, Crm, Dox, or Ama treated for 72 hours. The dead cells were harvested and then cocultured with BMDCs at a ratio of 1:5. After 24 hours, the dead cells were removed, and new medium was refilled. The BMDCs were stimulated with LPS (20 ng/ml) as a positive control. Data are depicted as box and whisker plots with whiskers showing minimum to maximum reported concentrations. All bars were compared to the mock bar. Statistical analysis was conducted by one-way ANOVA with Turkey's test for correction. $N = 3$ repeats. (**E**) C57BL/6 mice were vaccinated with cytotoxicant-treated EO771 tumor cells and rechallenged with live untreated EO771 tumor cells. Control mice received an equivalent volume of phosphate-buffered saline as a control. Overall survival was recorded after rechallenge. Statistical analysis was conducted by log-rank (Mantel-Cox) test for animal survival. n.s., not significant. $^{**}P < 0.01$, $^{***}P < 0.001$, and $^{****}P < 0.0001$.

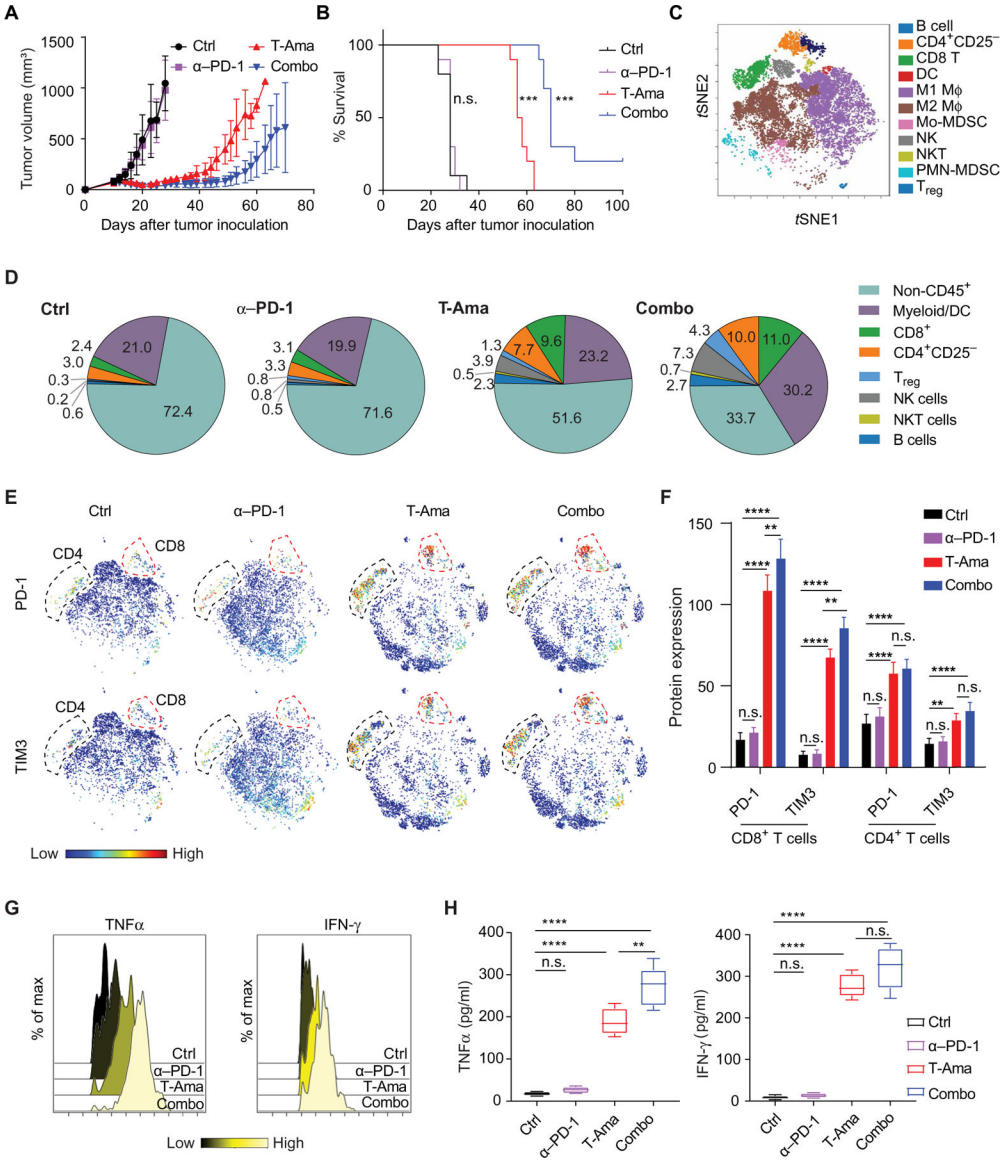


**Fig. 6. T-Ama potentiates immune checkpoint blockade therapy in treating HER2-low breast cancer.**

(**A** and **B**) Tumor growth curve (A) and survival analysis (B) in the C57BL/6-Tg(WapHER2) mice orthotopically implanted with $1 \times 10^6$ HER2-low EO771 cells with 11B loss. When the tumor reached 75 to 100 $mm^3$, the mice were randomized to four groups ($n = 10$ mice per group) for intraperitoneal injection with: (i) trastuzumab (20 mg/kg) (ctrl group) on days 7 and 14; (ii) T-Ama (5.0 mg/kg) on days 7 and 14; (iii) anti-mouse PD-1 (10 mg/kg) on days 5, 7, 9, 12, and 14; and (iv) combo treatment, T-Ama (5.0 mg/kg) on days 7 and 14 and anti-mouse PD-1 (10 mg/kg) on days 5, 8, 10, 13, and 15. (**C** and **D**) Analysis of the immune profile and microenvironment of mouse tumors derived from HER2-low/11B loss E0771 cells with the treatment as in (A) by CyTOF. *t*SNE (*t*-distributed stochastic neighbor embedding) representation of the immune cell subtypes after SPADE clustering is shown in (C) and mean percentages of distinct immune cell populations in the tumors are shown in (D). Mϕ, macrophage; NKT, natural killer T cells; DC, dendritic cells; Mo-

MDSCs, Monocytic Myeloid-Derived Suppressor Cells; PMN-MDSCs, polymorphonucler myeloid-derived suppressor cells; $T_{reg}$, regulatory T cell. (**E**) Analysis of PD-1 and TIM3 expression on $CD4^+$ (black dashed line circled) and $CD8^+$ (red dashed line circled) T cells from mice treated as in (A). (**F**) Quantitative data analysis of (E). (**G**) Expression of TNFα and IFN-γ from the infiltrating $CD8^+$ T cells was analyzed by CyTOF. (H) Intratumoral $CD3^+$ T cells from the tumors of the mice treated as in (A) were isolated, cultured ex vivo, and analyzed for the concentration of secreted TNFα and IFN-γ by ELISA. $n = 5$ replicates. For statistical analysis, one-way ANOVA with Tukey's test for correction was used in (**H**), two-way ANOVA test with Tukey's test for correction was used in (F), and log-rank (Mantel-Cox) test was used in (B). n.s., not significant. $^{**}P < 0.01$, $^{***}P < 0.001$, and $^{****}P < 0.0001$.